MESOSCALE MODELING AND ANALYSIS PERTINENT TO ELECTRODE PROCESSING

A Thesis

by

SESHENDRA PALAKURTHY

Submitted to the Office of Graduate and Professional Studies of
Texas A&M University
in partial fulfillment of the requirements for the degree of

MASTER OF SCIENCE

Chair of Committee,	Partha P. Mukherjee
Committee Members,	Debjyoti Banerjee
	Perla Balbuena
Head of Department,	Andreas A. Polycarpou

May 2016

Major Subject: Mechanical Engineering

ABSTRACT

Fabricating devices consisting of nanoparticles is a manufacturing challenge for novel small scale devices, e.g., ultrathin porous electrodes. Techniques that can have exquisite control over the shape, size and surface properties of nanoparticles have been developed. The efficient utilization of these highly functionalized nanomaterials is dependent on the assembly behavior and resultant microstructures. Evaporation-influenced nanoparticle assembly is a promising scheme to fabricate predefined microstructures.

In the present study, a morphologically detailed mesoscale model is developed to investigate microstructure variation produced by evaporation-influenced nanoparticle aggregation. Three dynamic processes, namely solvent evaporation, nanoparticle diffusion and rotation, are incorporated in the model. Fundamentally, system dynamics is dictated by the Hamiltonian, which is the function of interparticle, particle-solvent and solvent-surroundings interactions. Irregularity in particle shape is simulated by using hexagonal particles.

Aggregation characteristics like cluster size, film thickness and nanoparticle distribution are found to be a strong function of relative strengths of interaction energies. For evaporation-induced aggregation, an appropriate evaporation rate can facilitate nanoparticle aggregation. However, very high evaporation rates lead to a highly porous structure due to fast bubble growth.

Though the usage of nanoparticles for the electrodes has become the center of research, most of the batteries are still prepared using the micro-sized active particles. A Stratification model is used to predict the distribution of micro-sized active particles and KMC method is used to predict the distribution of secondary nanoparticles like conductive additives and binders on the active particles. The stratification model predicts that at lower Peclet number, a uniform film is formed. Also at higher Sedimentation number, particles deposit at a higher rate leading to uniform film formation on the substrate.

The KMC model predictions qualitatively explain morphological properties of a nanometer sized film of particulate slurry processed at different drying temperatures. The present simulations demonstrate that the higher drying temperatures and lower chemical potentials produce more compact film with less structural and surface inhomogeneities.

This work provides guidelines for the design of efficient microstructure manufacturing strategies. In addition, the developed framework can be easily extended to study realistic slurry behaviors, e.g., polydispersed solution and morphological variations of particles.

DEDICATION

I would like to dedicate this work to my family

ACKNOWLEDGEMENTS

I would like to thank my committee chair, Dr. Partha P. Mukherjee, and my committee members, Dr. Debjyoti Banerjee, Dr. Perla Balbuena, for their guidance and support throughout the course of this research.

Thanks also go to my friends and colleagues and the department faculty and staff for making my time at Texas A&M University a great experience. I also want to extend my gratitude to my mentors for guiding me through all the up and downs of my life.

Finally, thanks to my mother and father for their encouragement and love.

TABLE OF CONTENTS

Page

LIST OF FIGURES

Page

CHAPTER I

INTRODUCTION AND LITERATURE REVIEW

Li-ion batteries have conquered the market in various appliances like mobiles, laptops, automobiles [1-4], etc. because of its high specific capacity and energy density. Though the demands for these appliances are increasing, there is a scope for the improvement of its performance [5-10]. Some of the major areas which require the improvement are the low temperature performance, high discharge failures due to the formation of dendrites, and safety issues. In the quest to resolve these issues and to utilize the Lithium-ion batteries at a higher potential, lots of research has been focused on different areas. Li plating, dendrite formation, mechano-electrical degradation [11], microstructure of the Lithium ion batteries [12-18] and multi-scale modeling of nanoparticles assembly are some of the hot spots of the Li-ion battery research.

A recent review paper by Vu *et al*. [19], explained the benefits of using the porous materials for the electrodes. It has also discussed on various composite electrode materials and the properties of the electrodes like porosity, surface area and diffusivity of the Li-ions which depend on the microstructure of the electrode. From this, the importance of the microstructure of the electrode on the performance of the battery can be understood. The microstructure of the electrode depends on the fabrication mechanism [20-23], mixing sequence [24, 25] followed and the volume fraction of each constituent used in the electrode.

Fabrication of the electrodes

Fabrication of the electrode can be explained through 6 stages

1. Dry mixing: In the first stage, the active material like NMC is mixed with the conductive additive like carbon using a grinder. The mixture is grounded until we obtain a homogeneous mixture of constituents.
2. Wet mixing: In the second stage, a homogeneous solution of a solvent like NMP and the binder like PVDF is formed by stirring the solution for some time. Later, homogeneous slurry is prepared from the grounded mixture of NMC, Carbon black, and the homogeneous solution of NMP and PVDF by stirring them for some time.
3. Preparation of the substrate: An aluminum foil is taken and etched on both sides with isopropyl alcohol in a circular motion, with a Scotch-Brite Heavy Duty Scour Pad from the center towards the outside edges of the foil. This process is followed to improve the adhesion property of the aluminum foil by removing the Teflon residue present over the surface of the foil. Repeat the same procedure with the distilled water and isopropyl alcohol until no bending of the water occurs on the surface of the aluminum foil.
4. Film application: In this stage, the prepared homogeneous slurry is spread uniformly on the clean sheet of aluminum foil with the help of Elcometer.
5. Drying of the slurry: In this stage, the slurry spread on the aluminum sheet is dried at room temperature for some time, and then it is completely dried in the oven at a fixed temperature. After a while, the entire solvent present in the slurry gets

evaporated leaving a thin film of active material, conductive additive, and binder coated on the surface of the substrate.

6. Punching: Dried sheets are punched to prepare a thin film electrode of specific shape and size. The glove box is used to prepare a complete cell by combining the cathode with an anode and the separators.

During the fabrication of electrode, the major reason for insisting the mixture to be homogeneous is to remove chunks of the similar particle formed due to improper mixing. A homogeneous mixture improves the performance by providing the chance for individual particles to perform their functions. For example, the purpose of the binders is to bind all the other particles and the particles to the substrate. The purpose of the conductive additive is to improve the conductivity of electrons through the solid phase. The purpose of the active material is to provide the Li-ions. If the binders settle on top of the active particles then, the reaction at the surface of the electrode will be disturbed which results in the low performance. Similarly, flaking of the film is observed when the binders are not well-distributed as particles cannot stay attached to the substrate after the drying. Hence, they should be uniformly mixed at different stages. Etching of the aluminum foil should also be done carefully for a longer time to remove all the Teflon coating present on the surface of the foil. Etching improves the adhesion of the foil, which helps the binders to stick the particles to the surface of the foil.

Out of all the stages of the fabrication, the most complex sequence of actions takes place during the drying. It is a major stage where the particles self-assemble among themselves to form the microstructure. And the properties of the electrode depend on the

final microstructure formed at the end of the process. During the drying various processes like evaporation of the solvent, sedimentation, diffusion and rotation of the particles will take place. And various physicochemical chemical factors will affect each of these phenomenon and drive the self-assembly process.

Experimentally different types of methods and different compositions of the materials are used to fabricate an electrode. The drying of these thin film electrodes is a very slow process performed in an open air environment for a while and then carried out in an oven. Since it is a stochastic process observing how physicochemical factors affect the ordering or structuring of the electrode is a difficult task. Hence computational methods are developed to check the effect of different factors.

Literature review

Different scales can be used to analyze the microstructure of the thin film. Development of the thin film computational models with nanoparticles has been observed around the same time in both the continuum model as well as the mesoscale model. Some of the major contributions to the mesoscale model with self-assembly of nanoparticles are done by R. Rabani *et al.* [26-28].In the past decade, a lot of research has been going on in the self-assembly phenomenon to understand and get control over the process. Evaporation-induced self-assembly process is the most efficient mechanism proposed to replicate the self-assembly phenomenon by using the bottom-up approach. During the self-assembly of particles, the mechanism of thin film formation is driven by the evaporation of the solvent. As the evaporation proceeds, the particles resultant motion will be downwards and deposit over the surface of the substrate. The

evaporation of the solvent and the diffusion of the particles are the key parameters that decide the dynamics of the system. Since the dynamics of the system is random in nature, the method implemented to study this stochastic process should also account for this randomness. The details of the mechanism followed in the study are discussed later.

Aggregation of spherical and cubical nanoparticles with very small size and very high diffusivities, with different volume fractions [29], chemical potentials [30, 31], and interaction energies [32, 33] are the most emphasized parameters in the earlier studies. Recent studies have been focusing on novel fabrication techniques with different shapes like nanorods [28, 34, 35], heterostructures [34, 36], tetrapod's [37] and hollow particles [38], different shapes [39-46], aspect ratios [47-49], multi-phased nanoparticles [50], 3D assembly modelling [51, 52], solvents [53, 54], mobility of the particle etc. Some of the prominent works done include 3D lattice gas model [51], binary mixtures [50], rotation of the axisymmetric particles like nanorods [28], nucleation of the holes during the evaporation in wetting thin films [55]. Hydrodynamic thin film models [56-58] are developed to analyze the wetting layer formed over the surface of the nanoparticle. Despite the significant efforts made to get control over the self-assembly, our progress is not quite enough to get the complete control over the assembly. So still there is a need to understand and improve our models.

Min Zhu *et al*. modelled a non-spherical particle and developed an approach for calculating the interaction energy between species in Li battery electrode [59]. Fei Duan *et al*. also contributed with the study of coffee ring effect [29-31], where the branching phenomenon arises due to the evaporation of the droplet of senile nanofluid which is

similar to the study of thin film. Vancea *et.al* [60] has given a brief study of the branching phenomenon and the effect of chemical potential, diffusivity, volume fraction, interaction energies of the solvent and the particles on the aggregation phenomenon. Zhixiao *et al*. have studied the effect of different mixing sequences, different shapes and sizes on the aggregation phenomenon [61, 62].

Drying of the colloidal dispersions and latex film formation are the concepts which are very close to this study. In these studies, the particles concentration variation with respect to thickness and time are evaluated from the volume fraction of the particles in the solvent. The system is assumed to be continuous for deriving the governing equation required to solve for the volume fraction of particles. Sheetz *et al*. had proposed the non-uniform distribution of particles in the latex films and the skinning phenomenon [63]. Through these studies, the variation of porosity for different conditions in a latex film and the effect of different physicochemical factors in the formation of the thin film was reported. Davis, Russel *et al.* [64] and Auzerais *et al*. [65, 66] have solved a similar problem on sedimentation of the particles. Routh and Russel *et al.* [67-71] discussed the effect of the Peclet number on the vertical distribution of particles in the latex films. Shimmin *et al.* [72] proposed the inclusion of the sedimentation term in the latex films. Trueman *et al.* [73, 74] and Atmuri *et al.* [75] have recently developed a two particle stratification model and discussed the effect of Peclet number and interaction energies between the particles on the film formation.

Objective

The primary objective of this study is to understand the effect of different physicochemical factors on the microstructure of the electrode during the drying process. And the secondary objective of this study is to understand this effect at different length scales.

An attempt is made to analyze the drying of the thin film electrodes in a perspective to understand the distribution of particles at different scales. Microscale and mesoscale modeling and analysis is done to understand how particles interact with each other during the drying process, and the effect of physicochemical factors on the self-assembly phenomenon are studied. Over the past few decades, the active particles used in electrode fabrication are micro-sized particles. Hence, the analysis of the micro-sized active particles assembly in the presence of nano-sized binders and conductive additives is done. In the last decade, use of the nano-sized active particles in the electrodes has gained the attention to obtain higher efficiencies of the Li-ion batteries. But observing the limitations of their usage in the electrode fabrication, research has been going on to optimize their design as per the requirements. Keeping this in mind, an investigation is carried out on the hexagonal nano-sized active particles self-assembly and their interactions with the other species like binders.

CHAPTER II

METHODOLOGY

After the proper mixing of the slurry, a homogeneous mixture of particles with random position and orientation is obtained. The dynamics of the nanoparticles during the aggregation phenomenon follows a random walk in the lattice which depends on the various factors. One of the most efficient methods employed to reproduce such random walk is Monte Carlo method. Monte Carlo method (MC method) is an analytical method which deals with the random sampling techniques. In a purely statistical point of view, Monte Carlo method is defined as an art of approximating an expectation by the sample mean of a function of simulated random variables [76].

The above statement means the Monte Carlo simulation depends on the sampling technique followed to generate the random numbers. Generation of a random numbers is a difficult task. A sample of the random number is defined as a series of numbers which don't follow a sequence. Any sample of numbers generated by a technique will repeat after a while, which defies our purpose of generating random numbers. So it is impossible to generate a completely random number series. Hence, pseudo random number generator is used to generate the random number sample.

In general we have two sets of sampling techniques, Simple sampling and Importance sampling. Simple sampling technique deals with the equally distributed random number. Whereas, importance sampling technique uses weighted functions

random numbers by means of generation of Markov chains. A clear description of these techniques is given in various books [76, 77].

Generation of a pseudo random number

Pseudo random numbers are the sequence of numbers generated using a technique which satisfy the properties of a random numbers[78]. Lehmer proposed that pseudo random numbers can be generated by using a recurrence relation.

$$x_{i+1} = (ax_i + b)\left(modulo\, m\right)$$

Where a, b are the constants between [0 (m-1)] and m is the very large number in the order of 10^k. The remainder of modulo division gives the pseudo random number sequence. Normalizing these numbers gives the pseudo random number in the interval [0 1]. From the above equation it's clear that if k is a small number then the recurrence values will be observed after few numbers. Hence, the value of 'm' should be high enough to eliminate the repetition. This pseudo number generating model is also called as the congruential method or multiplicative congruential method.

Sampling techniques

Simple sampling

This technique is one of the simple Monte Carlo methods used to find the solution of the definite integrals which are intractable with the analytical methods. The solution of the integral form can be expressed analytically by calculating n desired equally distributed random numbers with a function in the interval [a b]. The fraction of the total number of hits taken by the random numbers multiplied by the area of the box formed by the interval gives the integral value.

$$I = \int_a^b f(x)dx \approx \frac{n_{hit}}{n}\left[h*(b-a)\right]$$

The larger the value of n the more precise will be the value of the integral. Approximate value of the integral can be expressed as

$$I = \int_a^b f(x)dx \approx \frac{1}{n}\sum_{i=1}^{n} f(x_i)$$

The statistical error of the integral is calculated based on the value of the variance of the function which is expressed as

$$\sigma^2(f) = \frac{1}{n}\int\left(f(x) - \langle f \rangle\right)^2 dx$$

$$\langle f \rangle = \int f(x)dx$$

$$\varepsilon = \sqrt{\frac{\sigma^2(f)}{n}}$$

where ε is the statistical error of the integral value of the function $f(x)$. The accuracy of the function can be improved by increasing the value of n or by decreasing the variance which decreases the statistical error.

Importance sampling

Importance sampling technique is developed to reduce the variance observed in the case of simple sampling technique by taking the weighted functions. The goal of this sampling technique is to distribute the random numbers in the areas of importance instead of distributing them uniformly throughout the interval as in simple sampling method.

$$I = \int_a^b f(x)\,dx = \int_a^b \frac{f(x)}{g(x)} g(x)\,dx = \int_a^b \frac{f(x)}{g(x)}\,dG$$

$$I = \frac{1}{n}\sum_{i=1}^{n} \frac{f(x)}{g(x)}$$

$$\sigma^2(f) = \frac{1}{n}\int \left(\frac{f(x)}{g(x)} - \langle f \rangle \right)^2 dG$$

$$\sigma^2(f) = \frac{1}{n}\int \frac{\left(f(x) - \langle f \rangle g(x) \right)^2}{g(x)}\,dx$$

The smartest choice of $g(x)$ would be proportional to $f(x)$, then the variance can be decreased to a small value thereby decreasing the error of the function.

Monte Carlo simulation can be divided into various types, some of the major methods are listed below.

Quasi steady state Monte Carlo method

Quasi-steady state Monte Carlo method is also called as crude Monte Carlo method[77]. It follows the simple sampling technique. A simple example of calculating the value of π is used to explain the method. Let us take $f(x) = x^2 + y^2$ in the interval [0, 1]. Using the simple sampling technique N uniformly distributed pseudo-random numbers are generated and plotted in the first quadrant. The number of hits of the random number is equal to the number of random numbers plotted inside the quadrant of the circle. The ratio of the number of hits to the total number of point, multiplied by the area of the square region gives us the area of the integral we are trying to find. In the example given

above in order to find the value of Pi, since we get the area of the quadrant we multiply the area with 4 and divide it by the square of the diameter of the circle.

Metropolis Monte Carlo method

Metropolis Monte Carlo method is one of the most efficient importance sampling techniques [79]. This technique uses the value of the weighted function $e^{-\left(\frac{\Delta E}{kT}\right)}$ as the probability of function to check the acceptance of the move. If each particle moves for n steps, then the total change in the energy of the system is considered as the average change in the energy of the system for every individual step. So Metropolis Monte Carlo method gives us an idea of how the energy of the system is changing with respect to diffusion steps of the particles. The system is said to attain equilibrium if the average change in energy of the system is negligible.

Kinetic Monte Carlo method

Kinetic Monte Carlo method is almost similar to Metropolis method [80, 81]. It follows the same algorithm but, the only difference is that here instead of taking the change of energy for the whole system it calculates the energy differences locally. Thereby reducing the time for the calculations and by counting the effect of diffusion of the particles on the system locally. When the average change in the energy of the system is very small, then the equilibrium of the system is said to be attained. The other specialty of KMC method is in solving the time dependent problems. For example rate of reaction in a system is given then the quantities after a certain time can be calculated using the KMC.

Methodology

In this project by considering the KMC-Lattice gas model we are trying to address the aggregation of the particles or deposition of the particles on the substrate during the drying phenomenon. The methodology we followed is explained by using flow chart below:

Algorithm of the model can be explained by dividing the above flow chart into two parts:

1. Initialization
2. MC process

In the initialization, we first generate the template of different particles. Using the center point of the each template created, we generate random points in the lattice which will be the centers of random particles generated. During the generation of the random particles, care is taken such that no two particles will overlap with each other. The next step followed is the relaxation of the binders.

In our model, the binders are soft polymers with chain-like structures. During the generation of the binder template, straight chain like structure is used for the ease of the geometry. After the proper mixing of the slurry, the orientation of the each link will be changed. And the entire structure looks disoriented.

The MC Process deals with diffusion and rotation of the particles as well as evaporation or condensation of the solvent. At each MC cycle, all the particles are checked for rotation. And diffusion of all the particles is checked for every MC step. The direction in which the particle can diffuse is a random process. Assuming the diffusivity as 1 in the

possible direction and rest as zero and multiplying the diffusivities by a random number, we can find the direction. The Sum of the diffusivities in all the four directions is subtracted with each diffusivity one after the other. The direction in which the difference becomes negative is the direction of diffusion. For the evaporation/condensation process, each cell in which either of the processes can happen is considered and checked for the phase transition. The dynamics of the system depends on the transition probability which can be calculated using the expression

$$P_{st} = \min\left[1, \exp\left(-\frac{\Delta H}{kT}\right)\right] \tag{2.1}$$

In the above expression k is the Boltzmann constant, T is the temperature of the medium and ΔH is the difference in the energies before and after the diffusion/rotation of the particle or evaporation of the solvent cell. The state of transition of is decided by comparing the transition probability P_{st} with a random number. The transition is accepted if and only if the random number generated is less than the transition probability. The position, orientation and lattice values of the particles are updated. Evaporation or condensation of the solvent cells also proceeds in a similar to the diffusion of the particles. Each MC cycle has M such steps. Each MC steps carries diffusion of the particles as well as evaporation or condensation of the solvent cell. The number of cycles depends on the final equilibrium state. When the slope of the total energy curve is less than 10^{-7}, the final equilibrium state is attained. Once the system attains the equilibrium, the diffusion of the particles and the evaporation rate of the solvent will be almost zero. At the ending step of the MC Process, preprocessing results are generated.

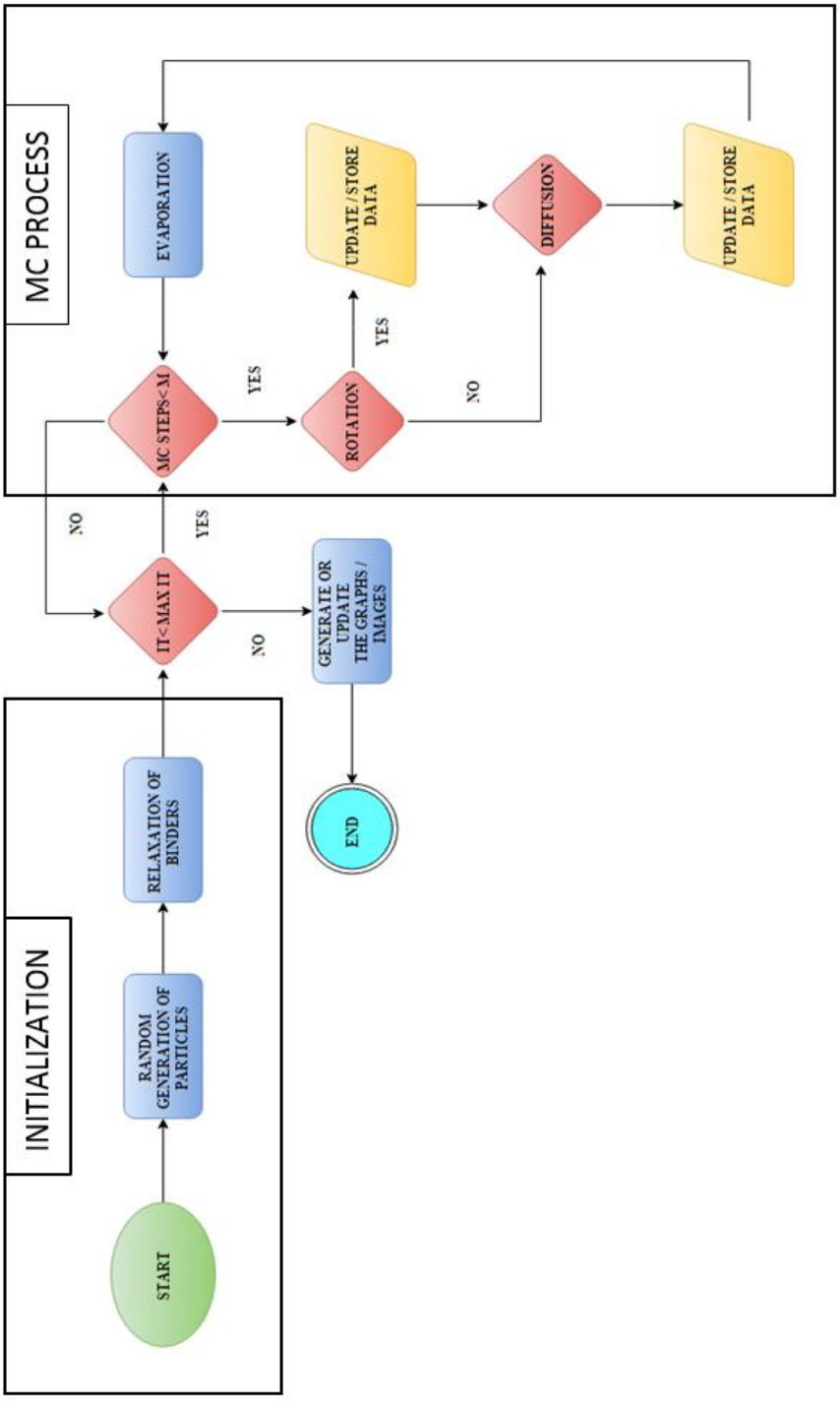

Figure 1: Flow chart of the method

CHAPTER III

STRATIFICATION OF ACTIVE PARTICLES AND DISTRIBUTION OF SECONDARY PARTICLES

In the previous chapters explanation for the fabrication of the thin film electrodes is given. Formation of thin films is shown through the microstructures in the following chapters by considering nano sized particles and their aggregation with the help of KMC method [43, 44, 82-88].

In this chapter the continuum model is considered with micro sized active particles and other secondary particles (conductive additives and binders) are considered to be as nano sized particles. Thin film electrodes formation and the effect of these nanoparticles on the micro sized active particles is studied by using the stratification model (continuum model) and KMC model. Stratification model is used to predict the volume fraction of the micro sized active particles along the height of the film and KMC model is used to predict the distribution of secondary particles on the surface of the active particles. In the stratification model the effect of the secondary particles is accommodated by the assuming higher values of viscosity. The scale of the model is $10^{-2}\ m$ but the nanoparticles are in the order of $10^{-9}\ m$ which is considerably very small when compared to the active particles of size $10^{-6}\ m$. The inertial effect of these nanoparticles is very small compared to the micro particles and can be neglected. So instead of considering the casted slurry as a multi-particle system, we have considered them as a part of solvent by increasing the

viscosity of the solvent which can affect both the diffusion of active particles and evaporation of the solvent.

Thin film electrode fabrication concept is similar to the latex film formation or colloidal dispersions where the particle are dispersed in the solvent and as the solvent dries the particles will be deposited over the substrate forming a thin film. Evolution of the microstructure is an interesting concept of the drying process. The arrangement of these particles during the drying plays an important role in deciding the properties of the electrode. This is achieved by finding the volume fraction of the active particles along height of the film. This approach is first developed by Kynch *et al*. by considering the sedimentation of the active particles. Later this technique was adapted by Rusell *et al.* in his book on colloidal dispersions. Brown et al and Zukoski *et al.* have made another wonderful contributions for the drying of thin films. Later Shimmin *et al.* added the sedimentation term to the equation derived by Brown et al. We have attempted to use the model given by Rusell *et al.* Brown *et al* and Shimmin *et al.* to find the volume fraction of particles with respect to space and time.

Dynamics of the system includes evaporation of the solvent and diffusion of the particles along with the sedimentation. So each of the process will be proceeding at parallel phases with evaporation decreasing the surface of the solvent film at a velocity E, particles exhibiting Brownian diffusion at a velocity V_D to eliminate concentration gradients and the sedimentation of the particles happening at a velocity of U. Since the thickness of the films is thin compared to the length of the film formed assuming that the distribution of particles is uniform along the length of the substrate conservation equation is considered

to be one dimensional in nature. Hence the velocities considered are all one dimensional in nature. The time scales of diffusion can be described by using the relation

$$t_{diff} \sim \frac{H_0^{\,2}}{D_0} \tag{3.1}$$

where H_0 is the initial height of the film and D_0 is the Stokes-Einstein diffusion coefficient. Considering the effect of secondary particles, α and β are the volume fraction of secondary particles in the pure solvent and effective solvent. Then both are related by the equation

$$\beta = \frac{\alpha}{(1-\phi)} \tag{3.2}$$

where ϕ is the volume fraction of active particles in the solvent. The effective viscosity of the solution and effective diffusion coefficient of the particles are given by the equations

$$\mu = \frac{\mu_s}{(1-\beta)^{2.5}} \tag{3.3}$$

$$D_0 = \frac{kT}{6\pi\mu R} \tag{3.4}$$

where k is the Boltzmann constant, T is the temperature of the system and R is the radius of the particle. And the evaporation scale is given by the relation

$$t_{eva} = \frac{H_0}{\dot{\mathrm{E}}} \tag{3.5}$$

where Ė is the evaporation rate of the solvent. These time scales can be compared with the help of a non-dimensional number called as Peclet number.

$$Pe = \frac{t_{diff}}{t_{eva}} = \frac{H_0 \dot{E}}{D_0} = \frac{6\pi\mu R\dot{E}}{kT} \tag{3.6}$$

The sedimentation of the particles is compared with the diffusion of the particles with a non-dimensional number

$$Pe_{sed} = \frac{H_0 U_0}{D_0} \tag{3.7}$$

where U_0 is the Stokes settling velocity of the spherical particles of radius R and density ρ_p in the solvent of effective density ρ and effective viscosity μ under the influence of gravity g.

$$U_0 = \frac{2R^2 g\left(\rho_p - \rho\right)}{9\,\mu_l} \tag{3.8}$$

$$\rho = \rho_\alpha \beta + \left(1-\beta\right)\rho_s \tag{3.9}$$

where ρ_α is the density of the secondary particles and ρ_s is the density of the pure solvent. The comparison between Pe and Pe_{sed} can be defined by another non-dimensional term called as sedimentation number.

$$N_s = \frac{Pe_{sed}}{Pe} \tag{3.10}$$

If N_s is greater than 1, then the evaporation is dominated by the sedimentation of the particles so the particles will be moving downward and based on the evaporation rate the distribution of the particles takes place at the surface of the film. If N_s is less than 1

then the evaporation of the solvent will be more than the sedimentation in this case uniform distribution of the particles can be observed than just depositing on the substrate. Cardinal *et al*. [89] has given a drying regime for all the three processes happening during the drying of a thin latex film. This gives an idea of which process plays a major role for a given parametric condition.

Governing equation and boundary conditions

1D conservation equation defining the particle volume fraction (ϕ) with respect space and time during the drying process can be expressed in the following way

$$\frac{\partial \phi}{\partial t} = -\frac{\partial J}{\partial y} \tag{3.11}$$

where left side term defines the rate of change of volume fraction and the right side defines the change of flux with respect to height of the film. Negative sign indicates the direction of the flux moving downwards due to the sedimentation. J is the flux of the diffusing particles given by the equation

$$J = -\left(U\phi + D\frac{\partial \phi}{\partial y} \right) \tag{3.12}$$

where U is the sedimentation velocity and D is the diffusion coefficient. They are defined by the following relations

$$D(\phi) = K(\phi)\frac{d}{d\phi}\left[\phi Z(\phi)\right] D_0 (1-\beta)^{2.5} \tag{3.13}$$

$$U(\phi) = K(\phi) U_0 \left\{ (1-\beta)^{2.5} \left[1 - \beta \left(\frac{\rho_\alpha - \rho_s}{\rho_p - \rho_s} \right) \right] \right\} \tag{3.14}$$

where $K(\phi)$ is the sedimentation coefficient which describes the hydrodynamic interactions, and $Z(\phi)$ is the compressibility factor which describes the concentration dependence of the osmotic pressure gradient.

$$K(\phi) = (1-\phi)^{6.55} \tag{3.15}$$

$$Z(\phi) = \frac{1}{(\phi_m - \phi)} \tag{3.16}$$

From the above equation it can be understood that $K(\phi)$ and $Z(\phi)$ are the strong functions of ϕ. ϕ_m is the maximum volume fraction. The specialty of the compressibility factor is that if the ϕ value comes close to ϕ_m, then the divergence of the function can be observed. So the form the equation plays an important role when the particles come close to each other during the collisions and maintains appropriate values. The maximum volume fraction chosen was $\phi_m = 0.64$. From the above discussion it should be noted that the spherical particles chosen are assumed to be hard spheres. The boundary conditions for solving the differential equation are at

$$y = 0; U\phi + D\frac{\partial \phi}{\partial y} = 0 \tag{3.17}$$

(No flux boundary condition) and at

$$y = H_0 - \dot{E}T; U\phi + D\frac{\partial \phi}{\partial y} = \dot{E}\phi \tag{3.18}$$

(Moving boundary condition)

By non-dimensionalizing the above differential equation we get,

$$\bar{t} = \frac{t}{\frac{H_0}{E}} \tag{3.19}$$

$$\bar{y} = \frac{y}{H_0} \tag{3.20}$$

$$\frac{\partial \phi}{\partial \bar{t}} = \frac{\partial}{\partial \bar{y}}\left[N_s A(\phi,\beta)\phi + \frac{1}{Pe} B(\phi,\beta)\frac{\partial \phi}{\partial \bar{y}} \right] \tag{3.21}$$

Non-dimensional boundary conditions used to solve the above partial differential equation are

$$\bar{y} = 0, \qquad N_s A(\phi,\beta)\phi + \frac{1}{Pe} B(\phi,\beta)\frac{\partial \phi}{\partial \bar{y}} = 0 \tag{3.22}$$

$$\bar{y} = 1 - \bar{t}, \quad N_s A(\phi,\beta)\phi + \frac{1}{Pe} B(\phi,\beta)\frac{\partial \phi}{\partial \bar{y}} = \phi \tag{3.23}$$

These equations are valid until the maximum packing fraction of ϕ_m is reached. Then the maximum dimension less time can be defined by

$$t_m = \frac{\phi_m - \phi}{\phi_m} \tag{3.24}$$

From the above boundary conditions it can be understood that upper boundary condition changes with respect to time. So in order to fix the upper boundary value with respect to time shrinking coordinate system is used. Then the shrinked coordinates become

$$\xi = \frac{\bar{y}}{(1-\bar{t})}, \tau = \bar{t} \tag{3.25}$$

Then the dimensionless conservation equation becomes

$$\frac{\partial \phi}{\partial \tau}+\frac{\xi}{1-\tau}\frac{\partial \phi}{\partial \xi}=\frac{N_s}{1-\tau}\frac{\partial}{\partial \xi}\left[A(\phi,\beta)\phi\right]+\frac{1}{Pe(1-\tau)^2}\frac{\partial}{\partial \xi}\left[B(\phi,\beta)\frac{\partial \phi}{\partial \xi}\right] \tag{3.26}$$

Boundary condition become

$$\xi=0,\quad N_s\,Pe\,A(\phi,\beta)\phi(1-\tau)+B(\phi,\beta)\frac{\partial \phi}{\partial \xi}=0 \tag{3.27}$$

$$\xi=1,\quad N_s\,Pe\,A(\phi,\beta)\phi(1-\tau)+B(\phi,\beta)\frac{\partial \phi}{\partial \xi}=Pe(1-\tau)\phi \tag{3.28}$$

Discretization

Implicit finite volume method is employed to discretize the equation. Time is discretized using the backward difference technique and central difference technique is used to discretize spatial grid. The solution to these equations is found by integrating over the control volume and using gauss divergence method to convert the control volume integral to surface integral. Control volume technique can be used since the spatial grid is fixed after using the shrinking coordinate system.

By using the gauss divergence theorem, we get that

$$\int_v \frac{\partial \phi}{d\tau}=\frac{\partial}{\partial \tau}\int_v \phi d\xi \approx \Delta\xi\frac{\partial \phi}{\partial \tau}\approx \Delta\xi\left(\frac{\phi_p^{p+1}-\phi_p^{p}}{\Delta\tau}\right) \tag{3.29}$$

The next term in the equation is a non-linear term, it is solved by using the differential rule

$$\int_v \xi\frac{\partial \phi}{\partial \xi}=\int_v \frac{\partial}{\partial \xi}(\xi\phi)d\xi-\int_v \phi d\xi \tag{3.30}$$

$$=\left(\xi\phi\right)_u-\left(\xi\phi\right)_l-\phi_p\Delta\xi \tag{3.31}$$

Similarly the other terms to the left hand side of the equation become

$$\int_\nu \frac{\partial}{\partial\xi}\left[A(\phi,\beta)\phi\right]d\xi=\left(A(\phi,\beta)\phi\right)_u-\left(A(\phi,\beta)\phi\right)_l \tag{3.32}$$

$$\int_\nu \frac{\partial}{\partial\xi}\left[\mathrm{B}(\phi,\beta)\frac{\partial\phi}{\partial\xi}\right]d\xi=\left(\mathrm{B}(\phi,\beta)\frac{\partial\phi}{\partial\xi}\right)_u-\left(\mathrm{B}(\phi,\beta)\frac{\partial\phi}{\partial\xi}\right)_l$$

$$=B(\phi,\beta)\left(\frac{\phi_u-\phi_p}{\Delta\xi}\right)-B(\phi,\beta)\left(\frac{\phi_p-\phi_l}{\Delta\xi}\right) \tag{3.33}$$

By putting all the equations into the parent differential equation we get that,

$$\frac{\Delta\xi}{\Delta\tau}\left(\phi_p^{p+1}-\phi_p^{p}\right)+\left[-\phi_p^{p+1}\Delta\xi+\xi\frac{\phi_u^{p+1}+\phi_p^{p+1}}{2}-\xi\frac{\phi_p^{p+1}+\phi_l^{p+1}}{2}\right]\frac{1}{\left(1-\tau^{p+1}\right)}$$

$$-\frac{N_s}{\left(1-\tau^{p+1}\right)}\left[A(\phi,\beta)\frac{\phi_u^{p+1}+\phi_p^{p+1}}{2}-A(\phi,\beta)\frac{\phi_p^{p+1}+\phi_l^{p+1}}{2}\right]$$

$$-\frac{1}{Pe\left(1-\tau^{p+1}\right)^2}\left[\left(B(\phi,\beta)\right)_u\left(\phi_u^{p+1}-\phi_p^{p+1}\right)+\left(B(\phi,\beta)\right)_l\left(\phi_p^{p+1}-\phi_l^{p+1}\right)\right]=0$$

(3.34)

On further solving the equation we get that

$$\phi_p^{p+1}\left[1-\frac{\Delta\tau}{\left(1-\tau^{p+1}\right)}+\frac{\Delta\tau}{2\Delta\xi\left(1-\tau^{p+1}\right)}\left[\left(\xi-N_sA\right)_u-\left(\xi-N_sA\right)_l\right]+\frac{\Delta\tau}{\left(\Delta\xi\left(1-\tau^{p+1}\right)\right)^2}\left(B_u+B_l\right)\right]$$

$$-\phi_l^{p+1}\left[\frac{\Delta\tau B_l}{Pe\left(\Delta\xi\left(1-\tau^{p+1}\right)\right)^2}+\frac{\left(\xi-N_sA\right)_l\Delta\tau}{2\Delta\xi\left(1-\tau^{p+1}\right)}\right]$$

$$-\phi_u^{p+1}\left[\frac{\Delta\tau B_u}{Pe\left(\Delta\xi\left(1-\tau^{p+1}\right)\right)^2}-\frac{\left(\xi-N_sA\right)_u\Delta\tau}{2\Delta\xi\left(1-\tau^{p+1}\right)}\right]=\phi_p^p \qquad (3.35)$$

Boundary conditions are discretized as follows

At $\xi=0$,

$$\phi_1\left(\frac{N_sA_1}{2}+\frac{B_1}{Pe\left(\Delta\xi\left(1-\tau^{p+1}\right)\right)}\right)+\phi_0\left(\frac{N_sA_0}{2}-\frac{B_0}{Pe\left(\Delta\xi\left(1-\tau^{p+1}\right)\right)}\right)=0 \qquad (3.36)$$

At $\xi=1$,

$$\phi_{N+1}\left(\frac{N_s A_{N+1}}{2}-\frac{1}{2}+\frac{B_{N+1}}{Pe\left(\Delta\xi\left(1-\tau^{p+1}\right)\right)}\right) + \phi_N\left(\frac{N_s A_N}{2}-\frac{1}{2}-\frac{B_N}{Pe\left(\Delta\xi\left(1-\tau^{p+1}\right)\right)}\right)=0 \tag{3.37}$$

Results and discussion

On solving the above discretized equations we get the variation of volume fraction with respect to height of the film and time. Important parameters which effect the evaporation, diffusion and the sedimentation in the system are Peclet number and Sedimentation number. From Figure 2 & Figure 3 we can understand the evolution of the volume fraction with respect to time. As the time passes, the height of the film changes and hence the volume fraction of the particles at the top surface has reached the maximum value. The effect of Pe and Pe_{sed} can be explained as follows, If the value of Pe <<1 then as per definition the evaporation of the solvent will be lower than the diffusion of the particles so the diffusion of the particles will be higher and the particle concentration will be uniform in the electrode. If Pe >>1 the evaporation takes over the diffusion. Because of the higher evaporation rate the gas front formed at the surface will move down at a faster rate and the particles appear to be at the gas and solvent interface. This is similar to higher chemical potential case with lower interaction energy between particles and the solvent. If Pe_{sed} <<1 then the evaporation is at the higher phase than compared to the sedimentation. Else if Pe_{sed} >>1, then the sedimentation is higher than the evaporation.

The effect of the Peclet number and Sedimentation number is shown the Figure 4. Each of these factors is varied while other being constant. At lower Peclet numbers due to the higher diffusion of particles over the evaporation we get uniform distribution of particles. Lower evaporation rates favor higher diffusion time for the particles. As the Peclet number increases we can observe that the volume fraction at the surface will reach the maximum value and the volume fraction at the bottom of the film will be lowered. This effect is due to the higher evaporation rates particles will not get enough time to diffuse and the growing evaporation front pushes the particles so higher volume fraction of particles will be present at the top while bottom remaining at the lower values.

The above results are observed at $N_s = 1$, i.e. sedimentation is very low. If the sedimentation of the particles is increased while keeping the Peclet number constant ($Pe = 5$) we get that the concentration of particles at the bottom of the film increases as the Sedimentation number increases. From the Figure 4 it can be seen that for a very high Sedimentation number the sedimentation of particles is so high that maximum volume fraction of particles is reached at the bottom of the film and then decreases with respect to the height of the film. At lower sedimentation numbers we can observe higher concentration of particles at the surface of the film and then it decreases with respect to the height of the film.

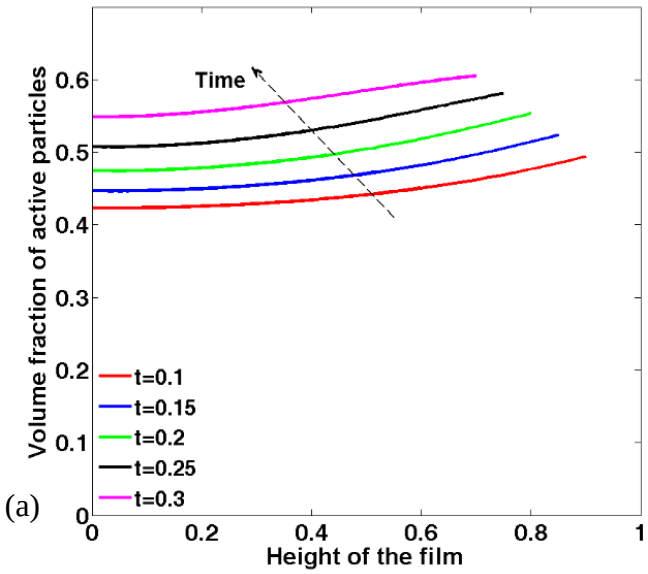

(a)

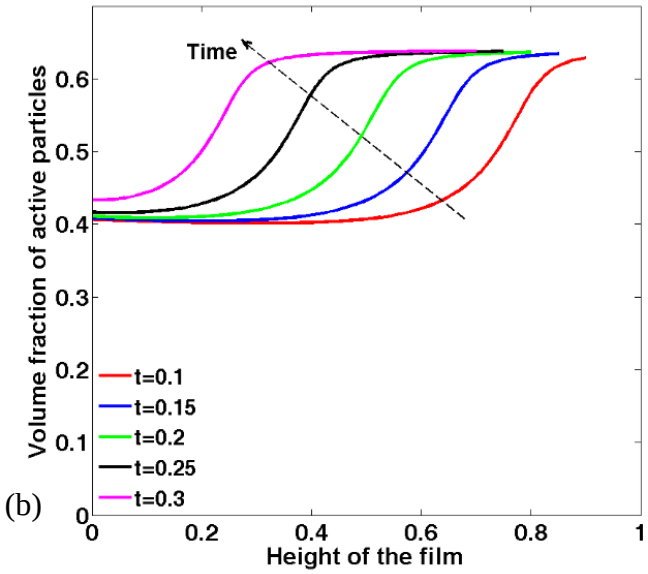

(b)

Figure 2: Evolution of volume fraction of active particles (a) $N_s = 1$ & $Pe = 0.1$ (b) $N_s = 1$ & $Pe = 1$

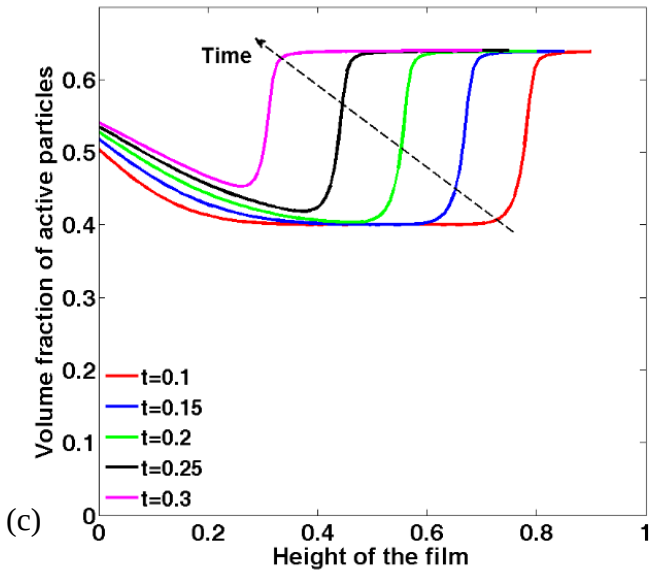

(c)

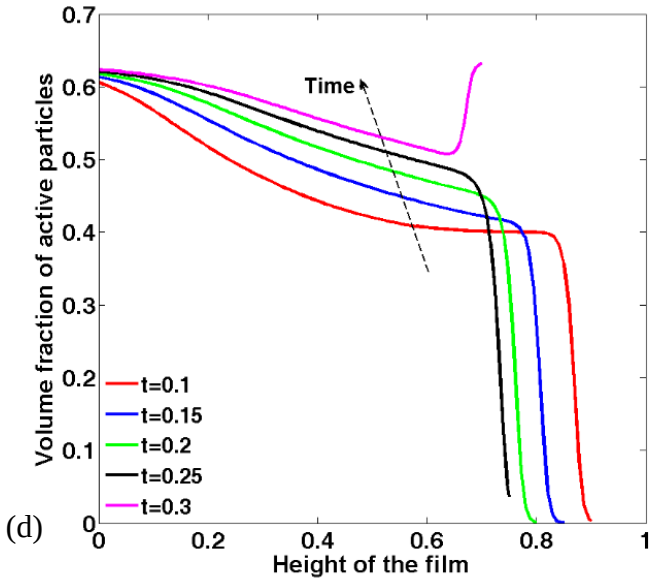

(d)

Figure 3: Evolution of volume fraction of active particles (c) $N_s = 10$ & $Pe = 5$ (d) $N_s = 50$ & $Pe = 5$

If the evaporation rate is very low compared to the sedimentation we can observe that concentration of particles decreases until surface of the film and then volume fraction of particles increases due to the particles present at the solvent and gas interface.

This model also accounted the secondary particles as the part of the solvent which increases the viscosity of the solvent. It is assumed that the distribution of these secondary particles is uniform throughout the solvent i.e. viscosity of the solvent is uniform throughout the solvent at a given time step. As the solvent volume fraction decreases with respect to time the viscosity of the solvent increases which slow down the diffusion and sedimentation of the active particles. So in this context the effect of viscosity also plays a major role in deciding the distribution of particles. From the definition of the effective viscosity it can be understood that, as the volume fraction of the secondary particles increases the viscosity increases.

Figure 5 shows the effect of initial alpha on the volume fraction of active particles evolution. On observing we can understand that as the alpha value increases the volume fraction of the active particles at the top surface increases and the volume fraction at the bottom of the film decreases. This is due to the increase in the viscosity, diffusion and sedimentation of the particles is lowered while the evaporation being unaffected. Due to the lower diffusion of particles and higher evaporation rate the volume fraction of particles at the gas and solvent interface increases. Due to the lower sedimentation of particles the volume fraction of the active particles decreases at the bottom of the film. With respect to time the effect of alpha on the volume fraction of particles also increases due to the increase in the viscosity of the solvent.

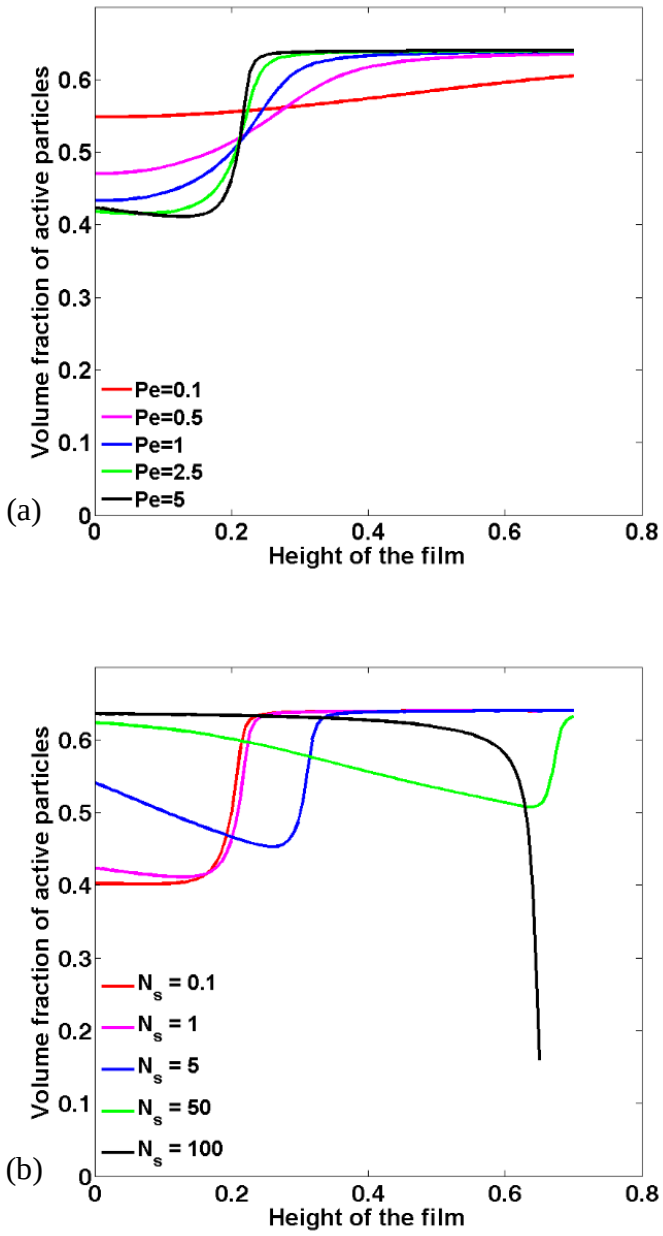

Figure 4: Effect of (a) Peclet number and (b) Sedimentation number on volume fraction of active particles

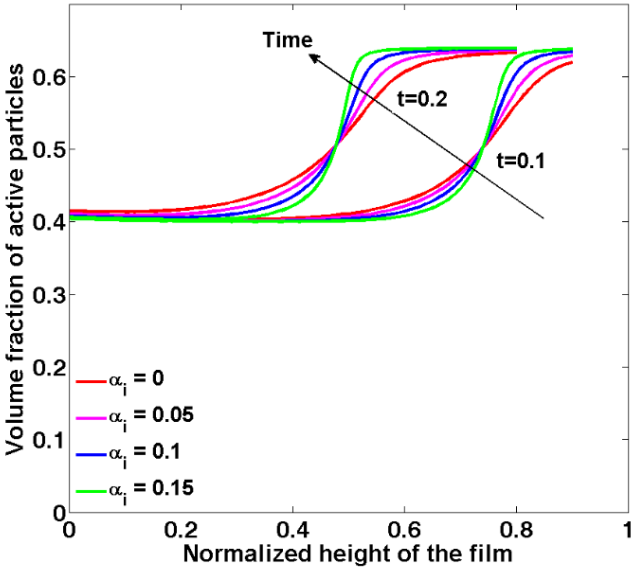

Figure 5: Effect of initial volume fraction of secondary particles (α_i)

Distribution of secondary particles

From the above discussion the distribution of active particles and the factors affecting them can be understood but during the drying even secondary particles will distribute upon the surface of these micros particles. Since they are considered as the part of the solvent using the continuum model their distribution over the surface of the active particles cannot be estimated. So by using a mesoscale KMC lattice gas model the distribution of secondary particles and the factors that affect them are studied. During the self-assembly process few of the possible scenarios of active particle assembly are considered for the secondary particle distribution. Figure 6 gives a clear idea of the three possible scenarios of self-assembly.

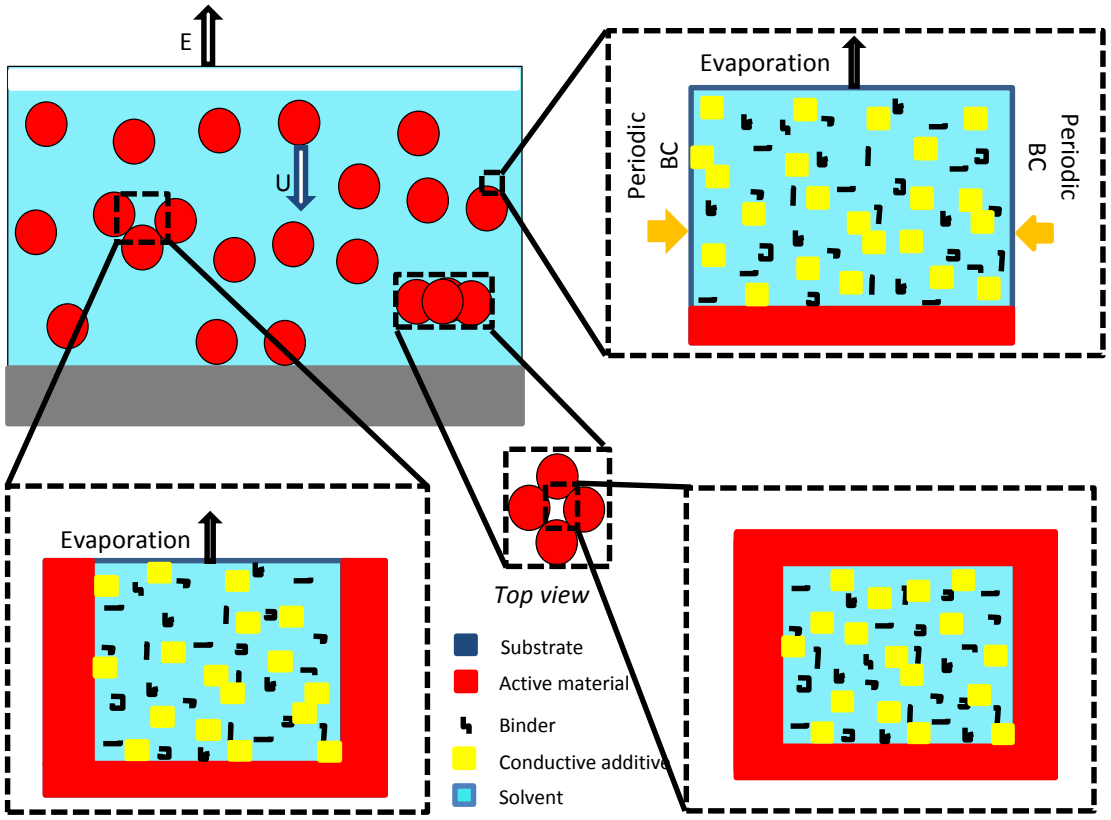

Figure 6: Possible scenario of active particle assembly

Distribution of secondary particles on the substrate is mainly effected by the chemical potential and temperature of the system. So in this study our emphasis was mainly towards these factors. In this case, we have assumed that the active particle surface to be flat in the small domain considered for the analysis. During the drying process the solvent gets evaporated and finally we can observe a thin film being formed over the surface of the active particles. The dynamics of the process includes both evaporation of the solvent and diffusion of the particles. Chemical potential is the driving force for the evaporation process and temperature effects both diffusion of particles and evaporation of solvent.

Figure 7, Figure 8 and Figure 9, explains us the effect of chemical potential and temperature on the microstructure for the single sided, three sided and four sided active particle surface. At a lower chemical potential the particles will diffuse for a very little time before which the increasing gas phase would push these particles towards the active particle surface. If the evaporation rate is slower than the diffusion, particles would get more amount of time to distribute in the lattice. The evaporation takes place from the top most cells of the solvent exposed to the gas phase. At higher chemical potentials and lower temperatures, since the evaporation and diffusion are slow the gas front proceeds at a uniform rate with particles diffusing downwards form the interface. As the chemical potential decreases the evaporation rate takes over the diffusion and fingered structures are formed. As the temperature increases diffusion of the particles increases due to which a film with uniform thickness is formed. At lower chemical potentials and higher temperatures diffusion as well as evaporation will be high so a uniform film with high packing fraction is formed.

From the final microstructures formed, at higher chemical potential and lower temperatures a film with less fingered like structures is formed as the chemical potential increases the number of fingers formed are increasing this is due to the less amount of time particles are getting due to higher rate of evaporation. As the temperature of the system is increasing the diffusion of particles also increases, but at $kT = 0.2$ number of fingers formed increases because the increment in the evaporation rate due to the increase in the temperature is higher than the increment in the diffusion of the particles. When the temperature increases even more then the diffusivity of particles will take over the

evaporation rate due to which diffusion dominates over the evaporation. At lower chemical potentials and higher temperatures diffusion and evaporation will be high and compact films are formed. At lower chemical potential and higher temperature condensation of the vapor happens at the surface due to the higher diffusion of particles at the surface.

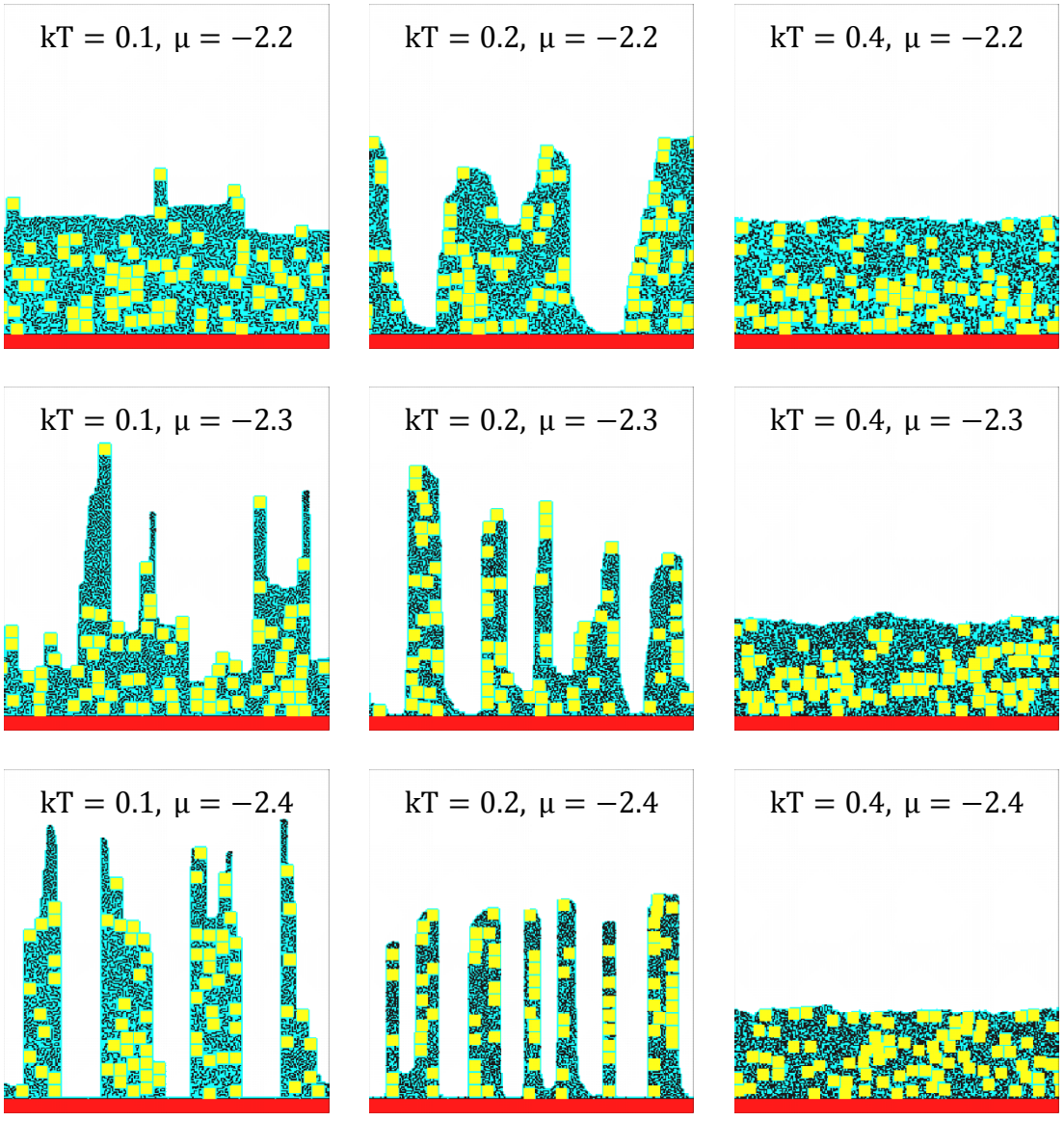

Figure 7: Final microstructure formed by the secondary particles on the surface of single sided substrate

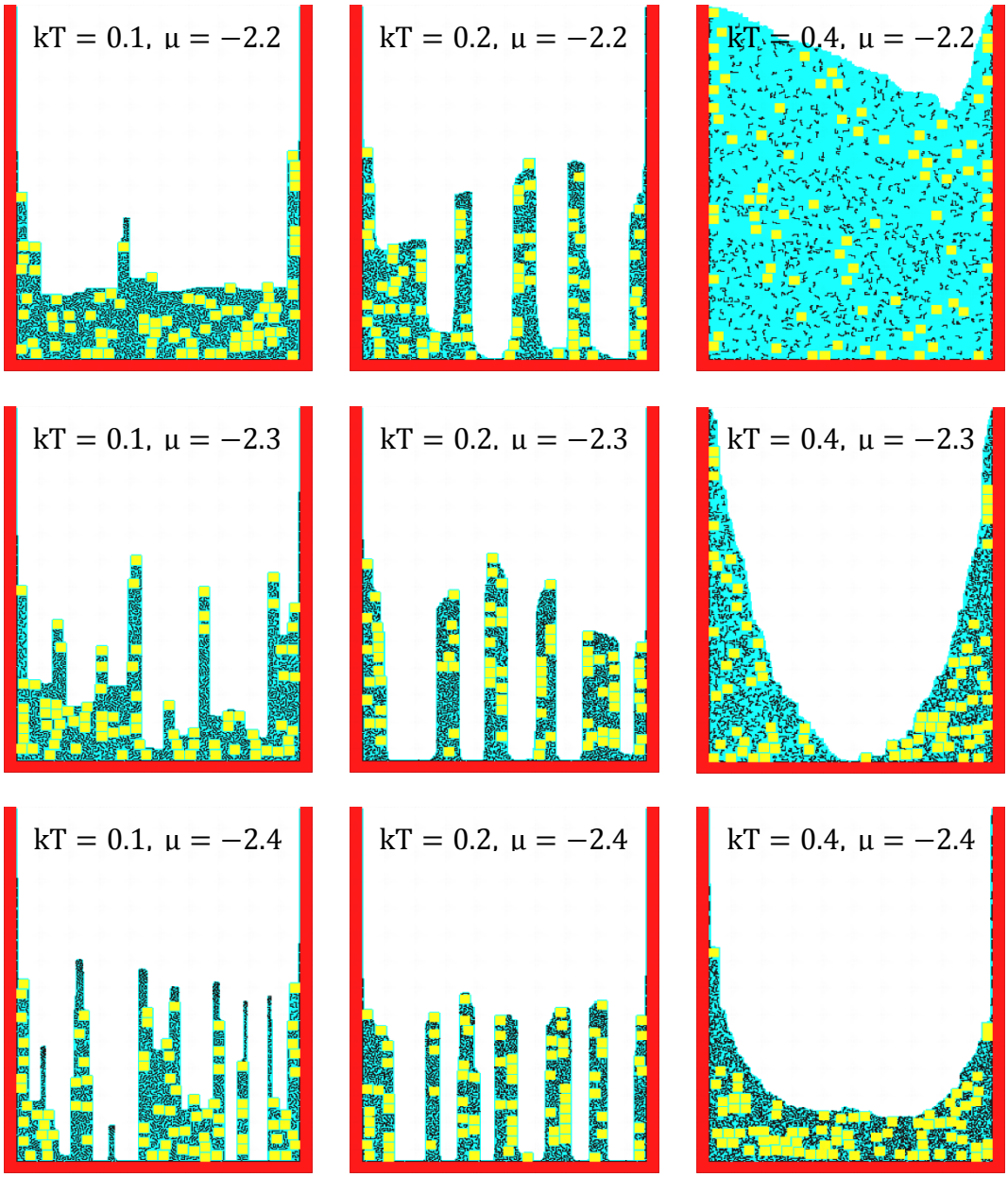

Figure 8: Final microstructure formed by the secondary particles on the surface of three sided substrate

In the case of four sided active particle surfaces the evaporation happens in Z direction (out of the film), by the formation of bubbles. Nucleation of the bubbles start at

random lattice cell once the threshold energy for the evaporation is reached. And the growth of the bubble depends on the interaction with the other cells. The effect of temperature and chemical potential on the system is explained through Figure 9. At higher chemical potentials and lower temperatures the evaporation of the solvent doesn't take place since the energy required for the growth of the bubble is not sufficient at lower chemical potentials. And since the evaporation takes more time initially the system is highly diffusive. Once the growth of the bubble starts it increases at a higher phase than diffusion. Then the diffusion is limited by the growth of the bubbles. At higher temperatures we can observe that the high diffusivity of the particles reduces the island formations. At higher temperatures the particles diffuse by condensing the gas phase around them, thereby forming a film over the surface of the active particles.

The above discussion gives us an idea of the film formed and what factors affect them during the drying process. Once the film is formed it is important to understand the characteristics of the film formed by evaporative induced self-assembly process. In order to understand the self-assembly process, contact area between the conductive additives and homogeneity of the binder distribution is found. In all the three cases studied, equal volume fraction of binders and conductive additives are considered. Since the volume (or area) occupied by the binder is less when compared to the conductive additives, binders are more in number than compared to the conductive additives. For the ease flow of electron, contact area between the conductive additives and the active particle should be more. And also contact area of binders with the active particles will definitely be more

when compared to conductive additives. Keeping in mind this issue we studied the conductive additives contact area with the active particle surface.

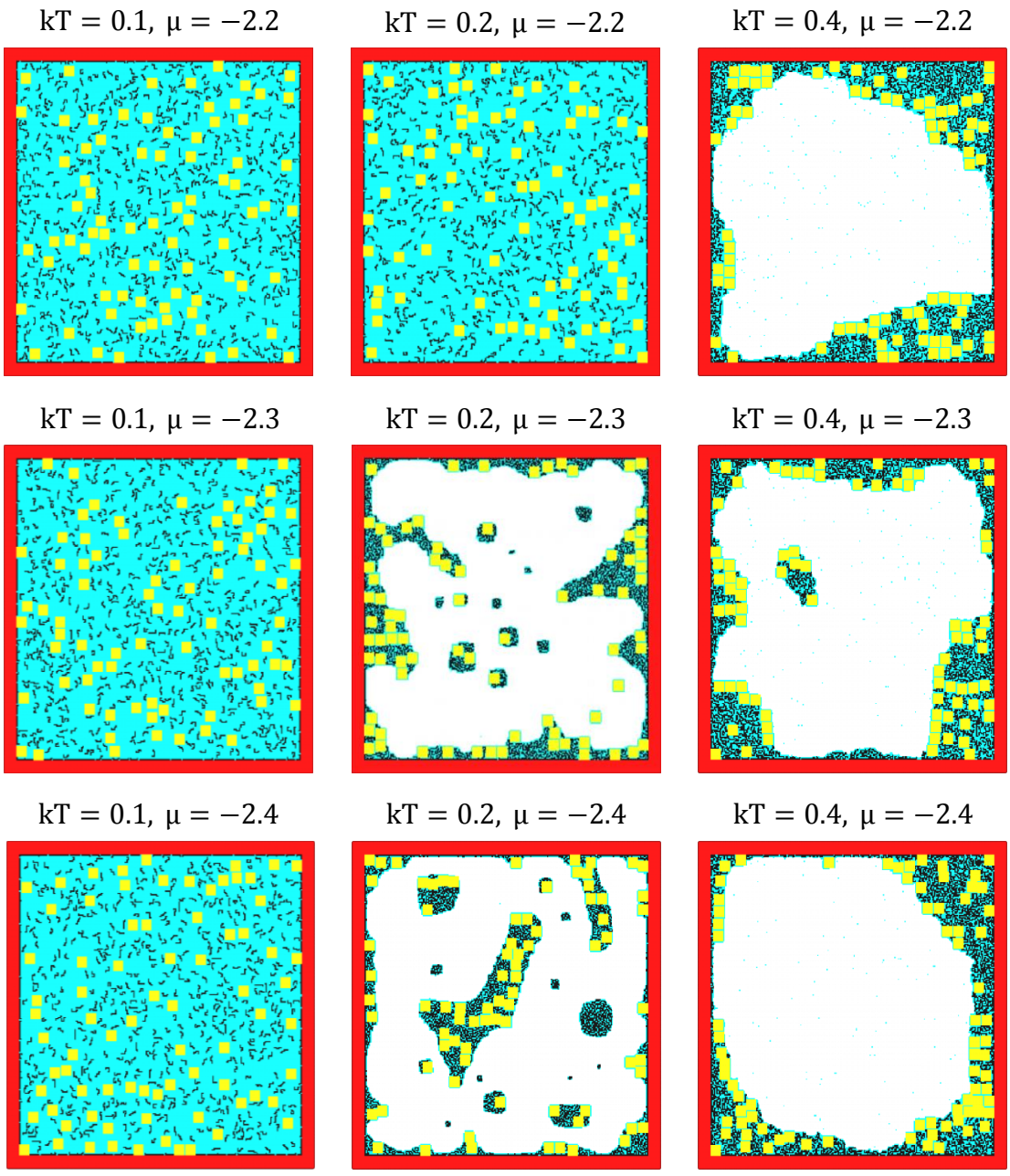

Figure 9: Final microstructure formed by the secondary particles on the surface of four sided substrate

Due to the lower number of conductive additives homogeneity of the conductive additives may not be enough to discuss regarding their distribution. So binder's homogeneity is only considered for this study. Figure 10-15 discusses about the variation of contact area of conductive additives with the surface of active particles and heterogeneity of binders with temperature and chemical potential.

From Figure 10 we can understand that the contact area of the conductive additives increases with respect to the chemical potential for $kT = 0.4$. This can be observed because, the increase in the diffusion of particles is more than the increase in evaporation rate. In the case of $kT = 0.1, kT = 0.2$ contact area increases and then decreases because at $kT = 0.2$, increase in the evaporation rate is higher compared to increase in the diffusion of particles. So particles are pushed to the surface there by contact area increases. The distribution of binders is analyzed using the heterogeneity index as shown in Figure 11, 13, and 15. Lower heterogeneity values represents more homogeneous distribution of binders in the system. From Figure 11, as the chemical potential is decreasing we can observe the heterogeneity values are increasing, i.e. the homogeneity of the system is disturbed with the increase in the evaporation rate. At $\mu = -2.2$ the heterogeneity index value for $kT = 0.2$ is higher because of the higher evaporation rate than the diffusion of the particles.

In case of three sided substrate, the contact area is higher at higher evaporation rates. This is due to the formation of columnar structures which push the particles to sides, thereby increasing contact area. If the diffusion of particles is high then the particles try to form a good film thereby increasing their concentration at the center of the film.

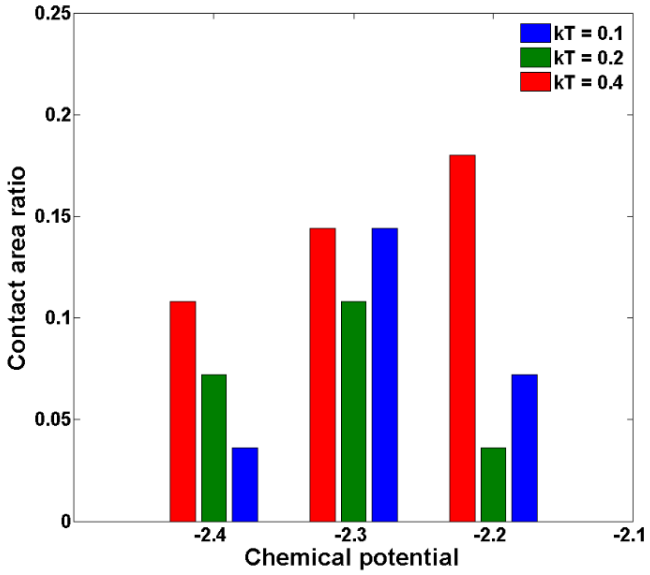

Figure 10: Effect of temperature and chemical potential on contact area ratio for single sided substrate

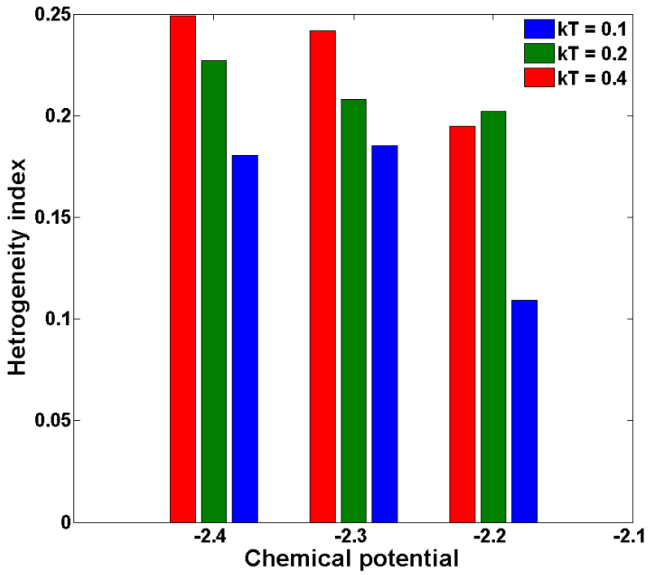

Figure 11: Effect of temperature and chemical potential on heterogeneity index for single sided active particle surface

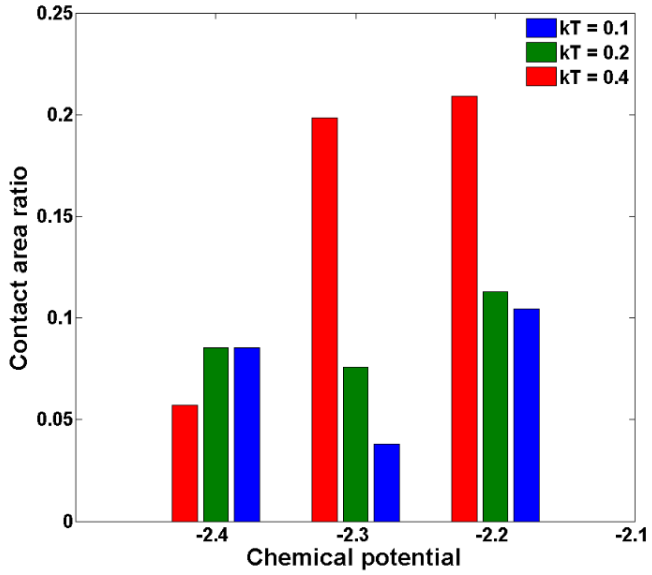

Figure 12: Effect of temperature and chemical potential on contact area ratio for three sided active particle surface

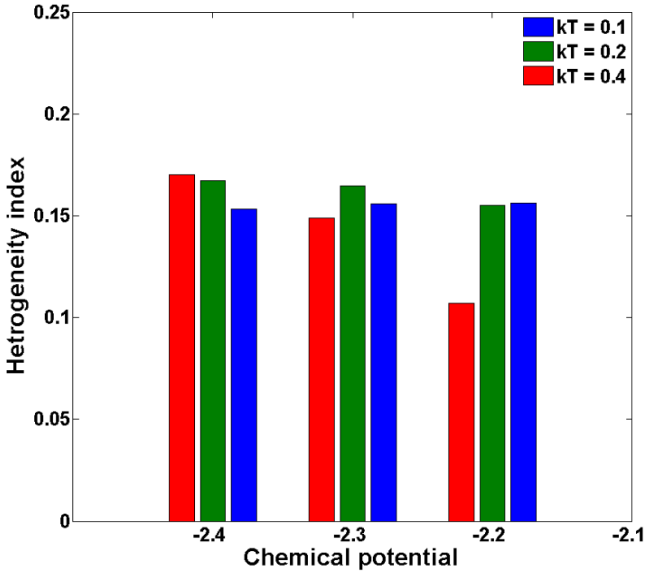

Figure 13: Effect of chemical potential and temperature on the heterogeneity index for a three sided active particle surface

From Figure 12, the contact area is maximum for lower chemical potential and higher temperatures similar to the one sided surface case. At lower chemical potential, the particles are pushed to the surface at a faster rate, so the binders present at the lower levels will not have enough time to diffuse to top which will deposit over the surface of active particle there by lowering the contact area. In the case of $\mu = -2.4, kT = 0.2$ and $\mu = -2.4, kT = 0.1$, due to the higher evaporation rate columnar structures formed create the higher contact area than in the case of $kT = 0.4$. Similarly, heterogeneity index also shows the minimum heterogeneity at higher diffusion scenarios. At $\mu = -2.2, kT = 0.4$ due to the condensation happening at the top surface more amount of solvent is left in the system which favors higher diffusion of particles. Hence more uniform distribution can be observed.

In the third scenario, since the evaporation is in Z direction all the particles will be pushed on to the active particle surface as the evaporation proceeds. In the cases of $kT = 0.2$, we can observe that the contact area is more than in case of $kT = 0.1$ because of the formation of islands and higher evaporation rates some of the surface area is free from binders for the conductive particles to deposit over surface of active particle. At higher temperatures due to the increased diffusivity of particles we can observe them mostly at the interface of gas and solvent. Similar to the previous cases the system is more homogeneous where the diffusion of particles is more, i.e. no evaporation cases. At $kT = 0.4$, we can observe that the heterogeneity is very high because of the fast growing evaporation front pushing the particles towards the surface of active particles. With respect

to the chemical potential the evaporation rate increases and heterogeneity also increases with evaporation rate.

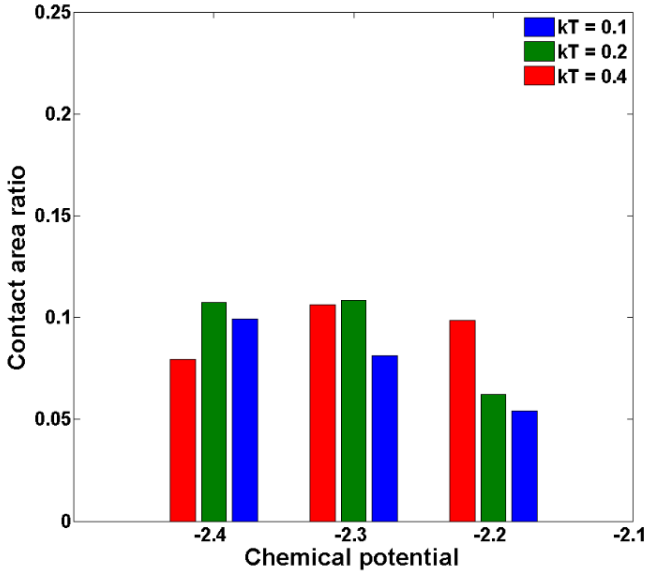

Figure 14: Effect of chemical potential and temperature on the contact area for a four sided active particle surface

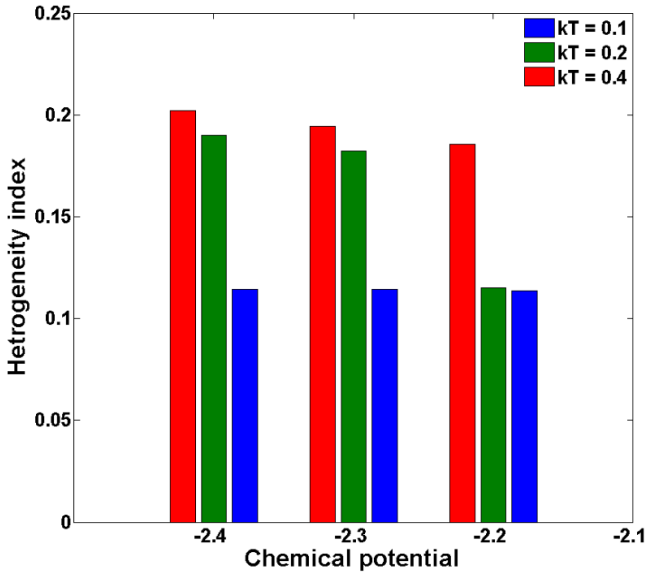

Figure 15: Effect of chemical potential and temperature on the heterogeneity index for a four sided active particle surface

CHAPTER IV

SELF-ASSEMBLY OF HEXAGONAL NANOPARTICLES

A 2D Coarse-grained Lattice gas model of size 500 X 500 is used to analyze the aggregation of hexagonal nanoparticles in a drying-mediated environment. The Kinetic Monte Carlo method is used to analyze the dynamics of the system. The domain is divided into identical lattice cells, the size of each lattice cell approaching the correlation length of solvent. Initially, each cell in the model is occupied by the solvent. Later some of the cells will be replaced by nanoparticles and as the dynamics of the system proceeds some of the solvent cells gets evaporated and occupied by gaseous cells. The iron rule of the model is: no two phases should occupy a single cell. So every cell is independent of other cells.

N numbers of hexagonal active particles are randomly generated in the system. The radius of the circumcircle passing through the vertices of the cyclic hexagonal particle i.e. 'R' is considered as the size of the particle. This study takes three different sizes of the particles R= 6, 8, 12 into consideration. The particles can exist only in one of the two directions possible since this is a lattice gas model. The particle can exist in the horizontal or the vertical state, i.e. represented by direction = 0 or 1. For the other states of the directions, the particles will be in the distorted shape.

As discussed in the previous chapter the dynamics of the system can be explained through the diffusion/rotation of the particles and the evaporation or condensation of the solvent cells/ gaseous cells. The diffusion of the particles is possible if the cells adjacent to the particle in a particular direction are occupied by the solvent. Similarly the rotation

of the particle is possible if the cells present inside the circumcircle and surrounding the particle are occupied by the solvent cells. Periodic boundary conditions are assumed for the boundaries in order to remove the edge effects. So if a particle crosses the boundary we can observe the other particle entering the system. The dynamics of the system depends on the probability of state of transition.

$$P_{st} = \min\left[1, \exp\left(-\frac{\Delta \mathrm{H}}{kT}\right)\right] \tag{3.38}$$

where ΔH is the difference in the energy of the states before and after the diffusion or rotation of the particle. And it is also called as the Hamiltonian. It is calculated by using the following energy expression

$$H = -\sum n_{ij}\varepsilon_{ij} - N_l\mu \tag{3.39}$$

$$\Delta \mathrm{H} = H_{final} - H_{initial} \tag{3.40}$$

In the above expression H is the energy at a state, n_{ij} is the number of i cells interacting with the j cells and similarly ε_{ij} is the interaction energy between i and j cells. Here i, j indicate the either of the phases solvent or gaseous or nanoparticle cells. N_l is the number of liquid cells present in the local structure and μ is the chemical potential of the solvent present in the system. ΔH is calculated by considering a local structure of size equal to (R+2) X (R+2) around the particle. Initially before the diffusion or rotation of the particle $H_{initial}$ is calculated and after the diffusion in the same local structure H_{final} is calculated. The difference in both the energies gives us the ΔH.

In this model, the value of ε_{ll} is considered to be as 1 and every other energy is represented in terms of ε_{ll}. The interaction energy between the active particles and the solvent (ε_{nl}) and interaction energy between the active particles (ε_{nn}) are considered as the parameters which affect the aggregation of the particles. Chemical potential (μ) is considered as the driving force for the evaporation of the system and Temperature ($kT = 0.3$) is considered as constant in this model.

In the methodology, it is mentioned that the particle diffuses by M steps for every iteration. The value M indicates the ratio of time taken for diffusion to the time taken for evaporation as indicated. So higher the value of M indicates higher the diffusion compared to the evaporation rate, i.e. it indicates the higher diffusivity coefficient. It also indicates the low viscosity of the solvent.

In this study, we would like to address how different physicochemical factors affect the formation of clusters and how two particles in a system interact with each other in a drying environment. The factors on which the equilibrium of the system depends are

1. Interaction energies
2. Chemical potential
3. Volume fraction of the active material (i.e. polyhedral particles)
4. Size
5. Temperature

Among these factors the size and volume fraction and temperature are not considered in our study. Since these quantities had already been studied by Rabani *et al.* group, we have considered the grid size and volume fraction of the particles from the

literature. The major factors are considered in this study are the interaction energies and chemical potential. Because these factors affect the aggregation behavior of the particles. In the following sections their effect will be clearly explained.

In general, the size or shape of the particle affects the final microstructure. We can observe that at a constant volume fraction of the active material present in the system as the size reduces the number of particles increases. This results in bigger size clusters but at the same time due to increasing in the number of particles we might also observe the lower average cluster size which in turn depends on the strong physicochemical factors. Through our observations, we find that there isn't much difference in the average cluster size evolution for R=6 and R=8. But we can observe a huge difference for R=12. We can also observe that due to the increase in the number of particles for lower sizes the rate of evaporation will be low due to the distribution of particles which in turn affect the interaction energies for the evaporation to take place.

The volume fraction of the active material present in the system also affects the aggregation of the particles. With the increase in the volume fraction, the average cluster size increases due to the increase in the number of particles. But due to high chemical potential or due to the higher interaction energies between solvent and particles, particles diffusion time might vary by reducing the average cluster size. So volume fraction and size of the particle alone give us an efficient conclusion about the aggregation phenomenon during the drying process.

The dynamics of the system consists of three steps:

1. Rotation

2. Diffusion
3. Evaporation

Evaporation of the solvent, Rotation & Diffusion of the particle depends on the probability of state transition. In calculating the probability of the state transition, we need to calculate the energetics using the Hamiltonian equation shown above. So, it depends on the interactions present between every two cells of the local structure. For rotation of the particle to take place the cells present inside the circumcircle around the particle should be occupied by the solvent. Similarly for the diffusion of the particle, cells adjacent to the particle in the direction of diffusion should be occupied by solvent cells. The difference in the energy form one state to the other is calculated by the Hamiltonian equation in the local structure around the particle. If the probability obtained is greater than the random number generated, the state transformation of the particle is accepted. Similarly for evaporation of the solvent, the change in the energy is calculated by the Hamiltonian equation in the local structure. So if the energy changes are high from one position to the other, the probability of state transition will be low. Hence, chances for the diffusion of the particle or evaporation of the solvent are low.

During the calculation of Hamiltonian in the local structure, if the sum of the interaction energies between two nanoparticle cells is more than the sum of the interaction energies between the nanoparticle and the solvent cells, then the diffusion of the particle might not happen. Due to the higher energy difference, the probability of transition will be low.

Similarly, if the interaction energy between the sum of the interactions between the nanoparticle and the solvent cells is greater than the sum of interaction energy between two nanoparticle cell interactions, then the chances for the diffusion of the particle are high. Since the probability of state transition for diffusion will be high. So the interaction energy between the particle and the solvent supports the diffusion of the particles in the solvent. And the interaction energy between the particles helps in the formation of clusters. Based on the interaction energies between the nanoparticle and the solvent, the process of self-assembly can be divided into two types, Spontaneous process and Evaporative induced process. In the spontaneous process, the interaction energy between the nanoparticle and the liquid will be low when compared to that of interaction energy between two nanoparticles.

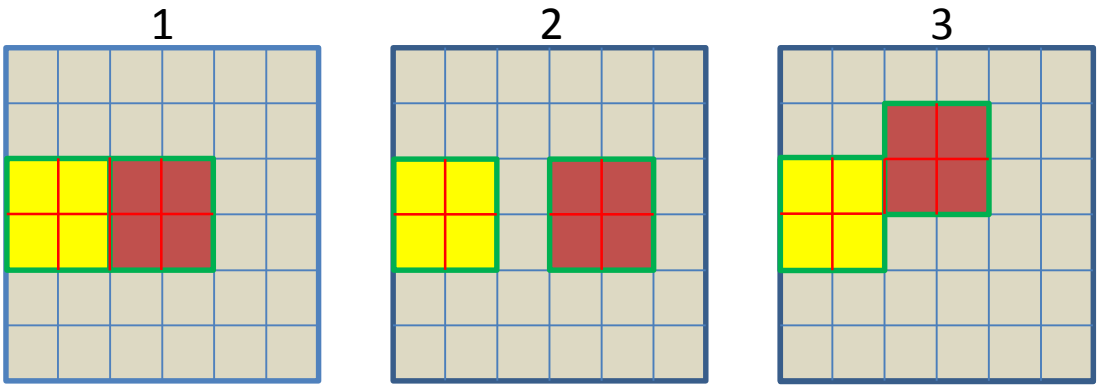

Figure 16: Explanation of interaction energy effect

Hence, diffusion of the nanoparticle is explained by the capillary forces i.e. due to the difference in cohesive and adhesive forces. Whereas in the evaporative induced process, the evaporated gas phase acts as the driving force and it pushes the nanoparticles to form a cluster as explained by Liu. Z *et al.*

Similarly, the evaporation of the solvent can also be visualized. The local structure for evaporation of a solvent cell consists of four cells surrounding from each side. The effect of interactions energies between the solvent cells in the no particle system will be lower than the overall value of the chemical potential in the local structure. Hence, the major contribution for the evaporation of solvent is the chemical potential. So chemical potential can be said as the driving force for the evaporation. Based on the evaporation rate the system can be divided into two types, homogeneous and heterogeneous system. In the homogeneous system, the evaporation rate will be high as the growth of bubbles occurs homogeneously throughout the domain. Whereas in a heterogeneous system, the evaporation rate will be low as the bubble growth happens randomly at few positions. Usually, this type of evaporation is headed with nucleation and growth of bubbles. And the nucleation sites are non-uniformly distributed in the domain. The prior studies by Rabani *et al.* and group also explains that the aggregation of particles varies based on the type of evaporation in the system. Hence, based on the interaction energies and chemical potential phase diagrams of average cluster size are constructed to find the dominance of each factor and their effect on average cluster size.

Phase maps

Phase map of average cluster size with respect to interaction energy (ε_{nn}) and chemical potential (μ)

From the phase diagram shown in Figure 17, the average cluster size first increase and then decreases with respect to interaction energy and the chemical potential. We can also observe that the average cluster size is symmetric about the diagonals of the rhombus.

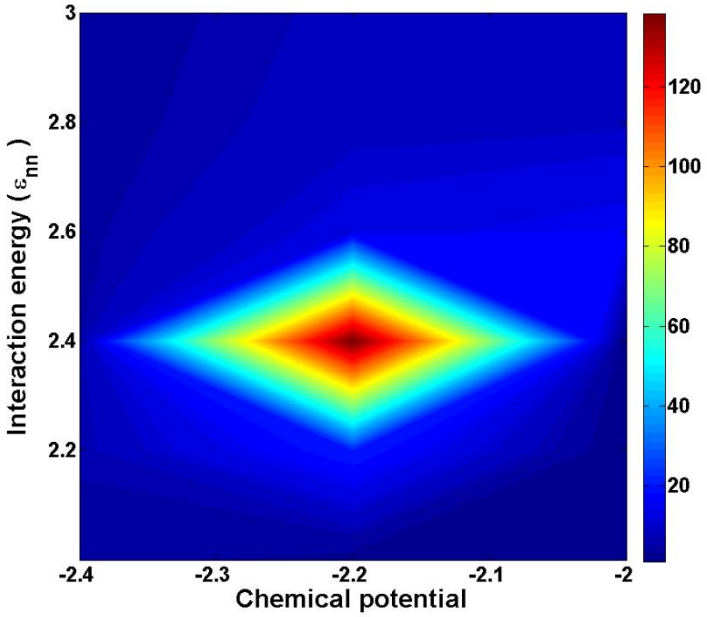

Figure 17: Phase diagram of average cluster size with respect to chemical potential (μ) and Interaction energy (ε_{nn})

For the clear understanding of the phase map we would like to discuss four aspects of the aggregation

Evolution of the average cluster size with respect to time

Initially, the particles in the system are distributed randomly throughout the domain. As the evaporation proceeds, due to the reduction of the solvent cells the diffusion of the particles slowly decreases tending towards almost zero. When all the particles seize to move, the system is said to reach an equilibrium state. As the dynamics of the system proceeds towards the equilibrium, clusters of the active particles are formed in the lattice. And the average cluster size increases with respect to time. After a while, we can

observe that the average cluster doesn't change much with respect to time but oscillates about a point.

Figure 18 shows that, for $\mu = -2.2, \varepsilon_{nn} = 2.4$ curve the average cluster size in the first phase increases rapidly and then it oscillates up and down. After a certain amount of time the system comes to an equilibrium state in which particles oscillate or diffuse locally in a few cells with respect to time. If the evaporation rate is low we can observe that the particles are surrounded by a film of solvent over them called as wetting layer. Due to the presence of this wetting layer, the particles will have a probability to move into these cells. Because of which the oscillation of the particles can be observed. If the chemical potential is low then due to the high evaporation rate the depletion of wetting layer is observed.

In the second phase, due to the oscillations of particles if one particle detaches from the big cluster the number of clusters increases because of which the average cluster size decreases. A similar case can be observed for $\mu = -2.2, \varepsilon_{nn} = 2.4$. In Figure 6 we can also observe that the average cluster size is low for other cases. This case is explained in detail while discussing the effect of interaction energy (ε_{nn}) and chemical potential(μ). The average cluster size shown in the phase diagram is represents the average cluster size at the end of the simulation.

Average cluster size variation with respect to chemical potential for different interaction energies

From Figure 19, it is clear that as the interaction energy increases the average cluster size also increases. After reaching a certain value it starts to decrease and reaches a minimum value. Previously, it is discussed that the ε_{nn} value helps in formation of

clusters. If the interaction energy between particles is high then the diffusion of the particle is limited by the particles which are in contact with that particle.

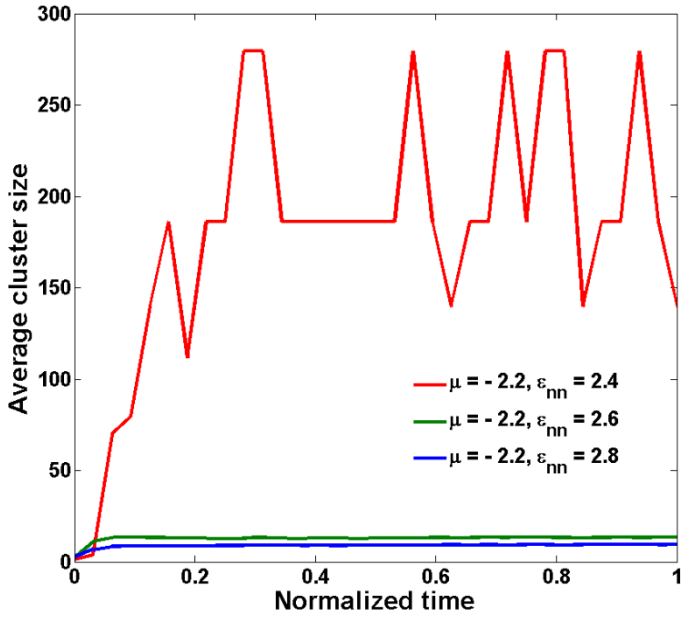

Figure 18: Evolution of average cluster size with respect to time

So as the interaction between the particles increases the average cluster size is expected to increase. But after a certain point, due to the high value of interaction energy between particles locally small clusters are formed. Hence, the diffusion of the particle is difficult because of the lower ε_{nl} value. Because of which the number of clusters increases, thereby reducing the average cluster size. If the chemical potential of the solvent decreases, the rate of evaporation increases. This in turn decreases the time for diffusion of the particles. Initially, the particles are randomly distributed in the lattice. If enough time is not provided for the particles to diffuse, due to the limited dispersion of particles the average cluster size is low.

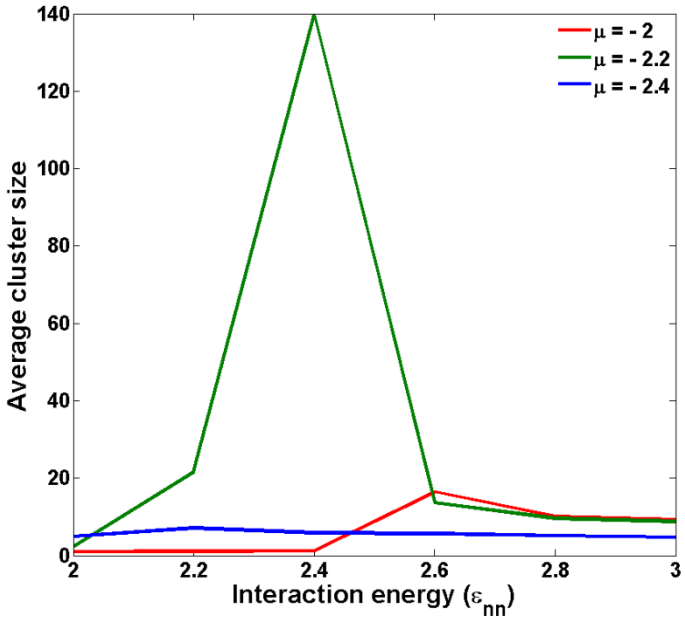

Figure 19: Average cluster size variation with respect to interaction energy (ε_{nn}) and Chemical potential (μ)

Final microstructure

Figure 20 shows the effect of chemical potential and interaction energies on the final microstructures. As discussed earlier for the solvent to evaporate in the system the chemical potential of the system should be lower than the critical chemical potential. The critical chemical potential of a no particle system is $\mu = -2$ [60]. Due to the increasing solvent cell interactions with the particles, the critical chemical potential of the solvent is lowered by the particles introduced into the system.

At $\mu = -2$, though some of the sites in the domain are free of particles the evaporation of the solvent cannot be observed. As the chemical potential decreases, the growth of the gaseous phase replacing the solvent cells is observed. It is also clear that,

as the interaction energy between the particles increases the cluster size increases and the compactness of the cluster formed is also clearly visible. The variation of average cluster size with respect to interaction energies can also be explained from these microstructures. For $\mu = -2.2, \varepsilon_{nn} = 2.4$ case, we can observe that the average cluster size is oscillating because of the red colored single particles joining the cluster and disjoining the cluster by diffusing into the solvent forming an independent cluster. At higher ε_{nn} values, the cluster of particles formed cannot disperse back into the solvent. It is because the energy of the particles will be low at maximum point of contact. If the particle disperse again into the solvent the interaction energy locally increases there by leading to the increase in the energy of the system. Since at lower energy system is more stable, the particles remain forming a cluster. Whereas in case of lower ε_{nn}values, the particle diffuses into the solvent to increase the interactions with the solvent cells. Thereby attaining the minimum energy state.

Contact area ratio variation with respect to chemical potential for different interaction energies

Contact area ratio is a very important parameter of discussion in case of electrodes. If two particles are in contact then the diffusion length of the Li ions increases thereby the resistance to the Li-ions also increases. So for an ideal case, we would always look for the lower contact area ratios. There are many other applications in which the area of contact plays an important role. The contact area ratio is defined as the ratio of the total contact area between every two active particles to the sum of total surface area of all the

particles. The contact area ratio gives us an information on the compactness of the microstructure.

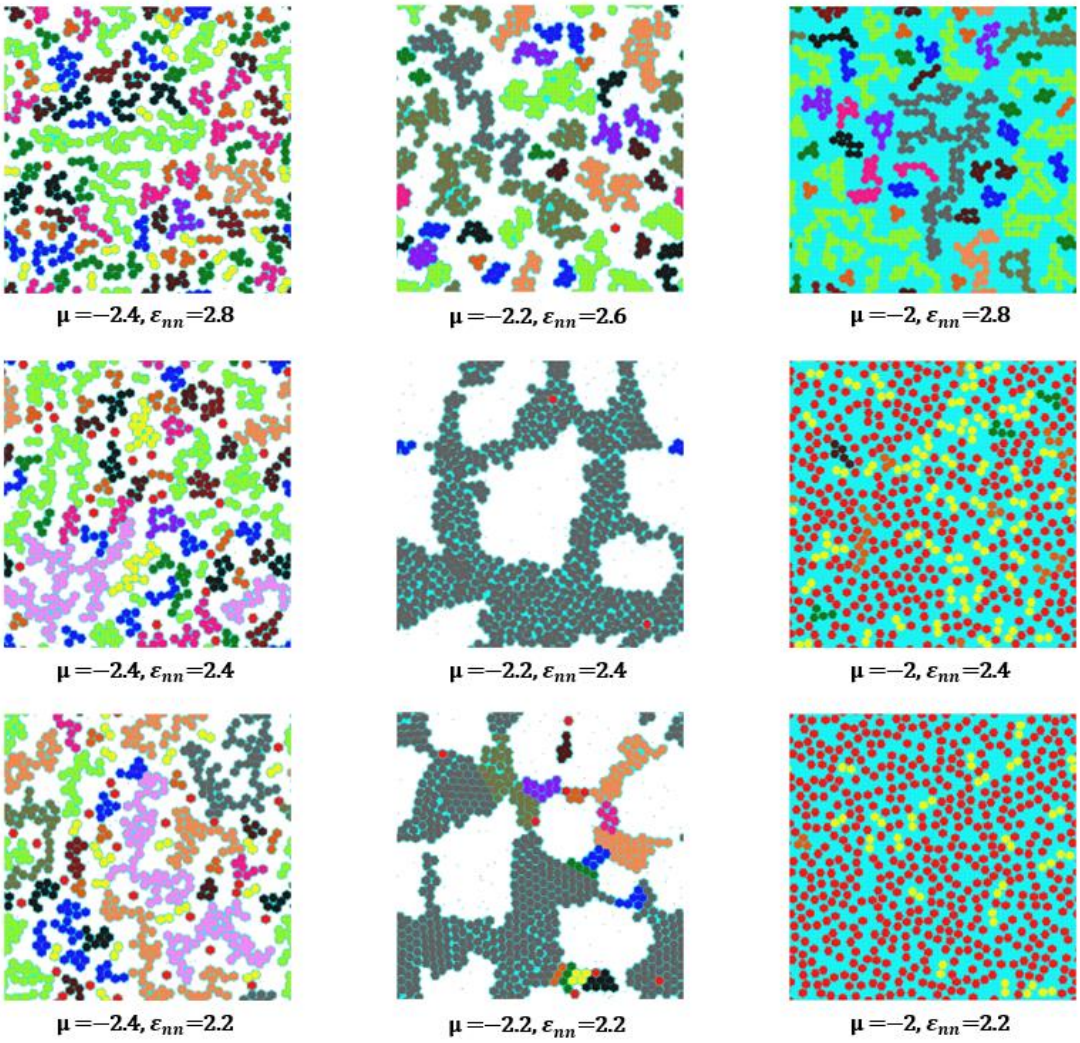

Figure 20: Final microstructures for different interaction energies (ε_{nn}) and chemical potentials (μ)

From Figure 21, we can understand that the area of contact increases with respect to interaction energy until the maximum possible area is achieved and then decreases. As the chemical potential decreases, the maximum contact area ratios also decreases. If the

average clusters size is maximum that doesn't mean that contact area ratio is at maximum. Because, in the case of maximum cluster size since the ε_{nn} values are not very high so the particles are covered with solvent around them. But for higher ε_{nn} values, we can observe a very high area of contact between the particles.

For achieving more compact structures we required to have diffusion which increases the contact area. Average cluster size and area of contact can be related to explain this phenomenon. As the average cluster size increases, the number of particles in contact also increases. With the increase in the number of particles in a cluster, the contact area increases. So the contact area ratio first increases with respect to interaction energy between particles and then decreases similar to average cluster size. But though the cluster size seems almost constant the area of contact can change from one cell to several cells. At higher evaporation rates achieving the maximum area of contact becomes difficult due to the fast growing gas front.

In Figure 22, the final microstructure obtained for different conditions are given. From the figure, we can clearly see that $\mu = -2.2, \varepsilon_{nn} = 2.4$ has the biggest cluster size but if we look at the particles, the area of contact is lower than compared to $\mu = -2, \varepsilon_{nn} = 2.6$.

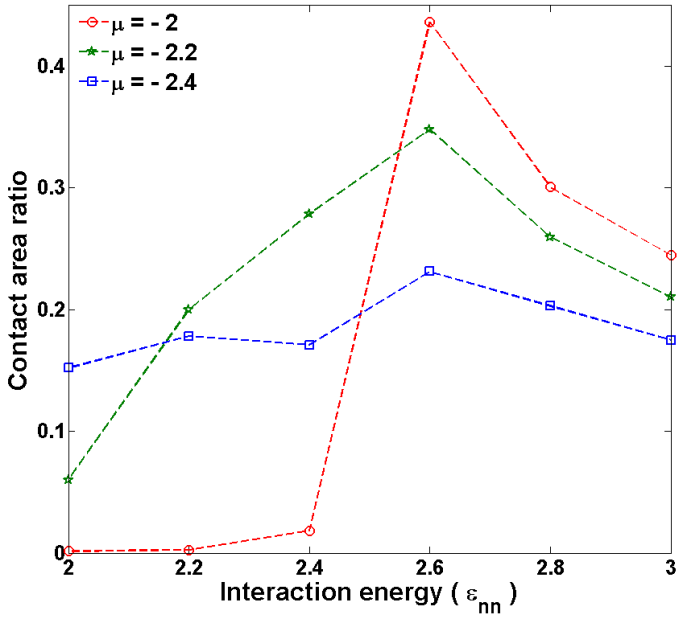

Figure 21: Contact area ratio variation with respect to the interaction energy (ε_{nn}) and chemical potential (μ)

Similarly, if we observe the particles in the $\mu = -2.2, \varepsilon_{nn} = 2$, case the particles are well aligned but we can see that they are separated by the solvent film which reduces the area of contact between particles. In the case of $\mu = -2.4, \varepsilon_{nn} = 3$ we can see that the number of clusters formed is more in number. Due to high evaporation rate and high ε_{nn} value the clusters formed are more compact in nature with high contact area than compared to the other cases with $\mu = -2.4$.

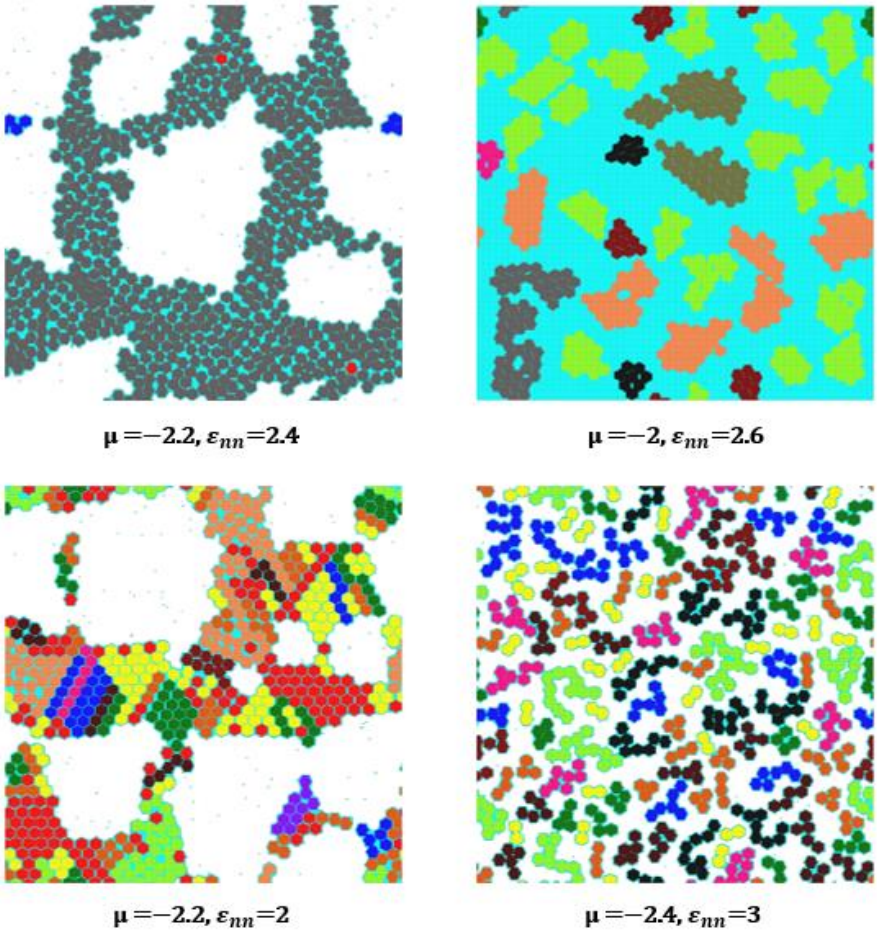

Figure 22: Microstructure at different points of contact area figure

Phase map of average cluster size variation with respect to interaction energy $(\boldsymbol{\varepsilon_{nl}})$ ***and chemical potential*** $(\boldsymbol{\mu})$

Similar to the first phase map, the average cluster size is maximum at the center and decreases as we go farther away from the center. But we can clearly observe that there are two layers with different properties. In the first layer, the average cluster size is very low. Whereas in the other layer we can observe that the average cluster size varies with respect to the interaction energy and chemical potential at a high rate. We can also observe

from the scale that the maximum average cluster size noticed is lower than in the case of ε_{nl} than compared to ε_{nn}.

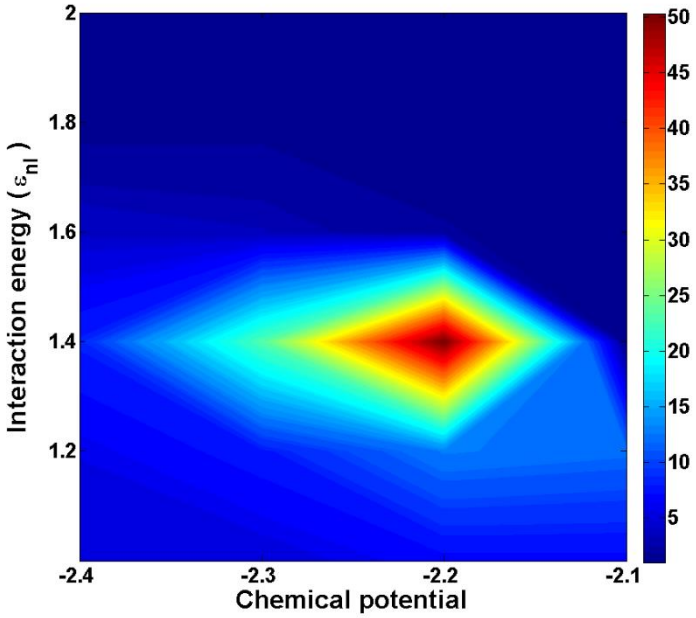

Figure 23: Phase map of average cluster size variation with respect to interaction energy (ε_{nl}) and chemical potential (μ)

As in the previous case we would like to describe the phase diagram with the help of four different aspects as follows:

Evolution of average cluster size with respect to time

As discussed previously, the evolution of the average cluster size in the case ε_{nl} will be same as the case of ε_{nn}. From Figure 24, it can be observed that the average cluster size first increases at rapidly and then it oscillates with a little increase. This is mainly due to the evaporation of the solvent in the system. Initially, there is a lot of solvent present in the system. As the evaporation proceeds, the solvent gets reduced and the chance for the

diffusion of the particles reduces. Because of the little solvent present in the system the particles diffuses thereby joining the cluster with the other particles and disjoining the clusters formed. It can also be observed that average cluster size increases and then decreases with respect to increase in ε_{nl} values.

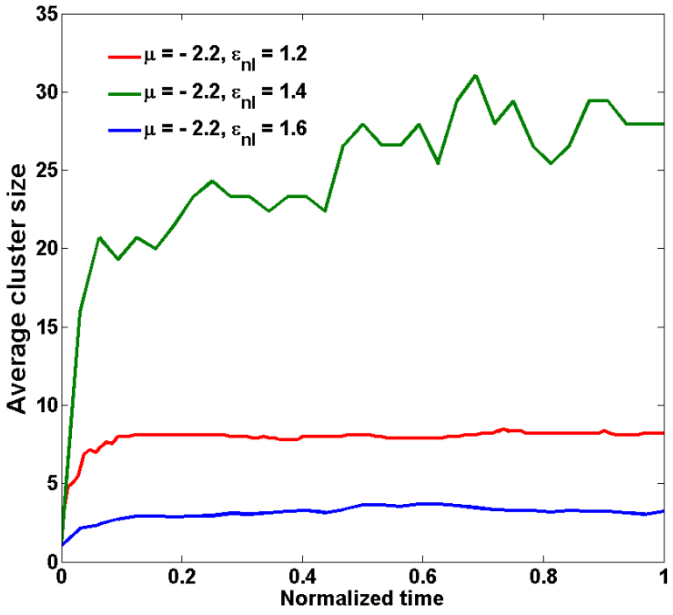

Figure 24: Evolution of average cluster size with respect to time

Variation of average cluster size with respect to interaction energy (ε_{nl}) and chemical potential (μ)

Figure 25 gives the information on the variation of average cluster size with respect to interaction energy. (ε_{nl}). In these simulations, we have considered ε_{nn}=1.7. Initially due to the higher ε_{nn}values and lower ε_{nl} values we can observe higher average cluster size. But as the ε_{nl} value increases the diffusion of the particles increases. Until the effect of ε_{nl} matches the effect of the ε_{nn} the average cluster size increases. Once the interaction

energy between the active particles is overcome by the interactions between solvent and particle the diffusion of the particles will dominate over the aggregation. Resulting in the decrease of the average cluster size due to the dispersion of the particles. If the chemical potential is low, since the nucleation happens at a faster rate due to the dispersed particles the aggregation of particles cannot happen in less amount of time.

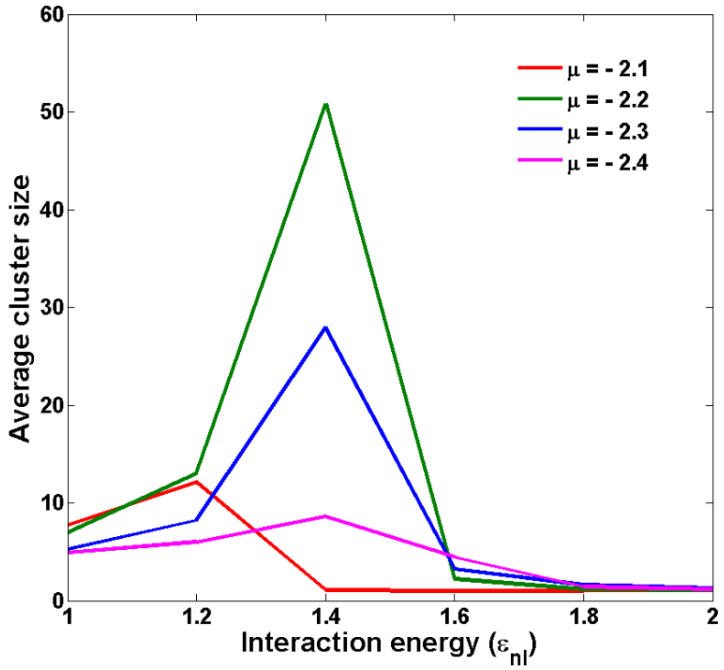

Figure 25: Variation of average cluster size with respect to interaction energy for different chemical potentials

So we can observe that as the chemical potential decreases the average cluster size also decreases. If the chemical potential is high then due to the higher time for the particles to disperse we can get a moderately high average cluster size for lower ε_{nl} values and at higher ε_{nl} values we can observe a lower average cluster size.

Final microstructure and its dependence on the ε_{nl} and μ

A much clear explanation can be obtained from the final microstructures in order to define the effect of ε_{nl} and μ on the system. From Figure 26, we can understand that the diffusion of the particles is low at the lower ε_{nl} values because of the higher ε_{nn} values because of which aggregation of particles takes place. At higher ε_{nl} values we can observe that the particles diffuse away into the solvent there by aggregation decreases. It can clearly be observed in the case of $\mu = -2.1$, the solvent is not evaporated completely because of the higher interactions of the particles with the solvent. As the chemical potential decreases we can observe that the solvent is evaporated but we can still observe the traces of solvent present in between the particles as a wetting film. This film gets stronger if the interactions between solvent and the particles increases.

Variation of contact area ratio with respect to ε_{nl} and μ

From the Figure 27, we can understand that similar to the average cluster size the area of contact increases and then decreases with respect to the increase in the interaction energy (ε_{nl}). From the previous discussion we can understand that, with the increase in the ε_{nl} value the diffusion of the particles increases. Though the average cluster size is maximum at $\varepsilon_{nl} = 1.4$, we can observe that $\mu = -2.1, \varepsilon_{nl} = 1.2$ has the maximum contact area ratio. Because of the low evaporation rate there is a maximum time for diffusion of particles and the effect of ε_{nn} is strong until $\varepsilon_{nl} = 1.2$, after that the diffusion is taking over the ε_{nn} value.

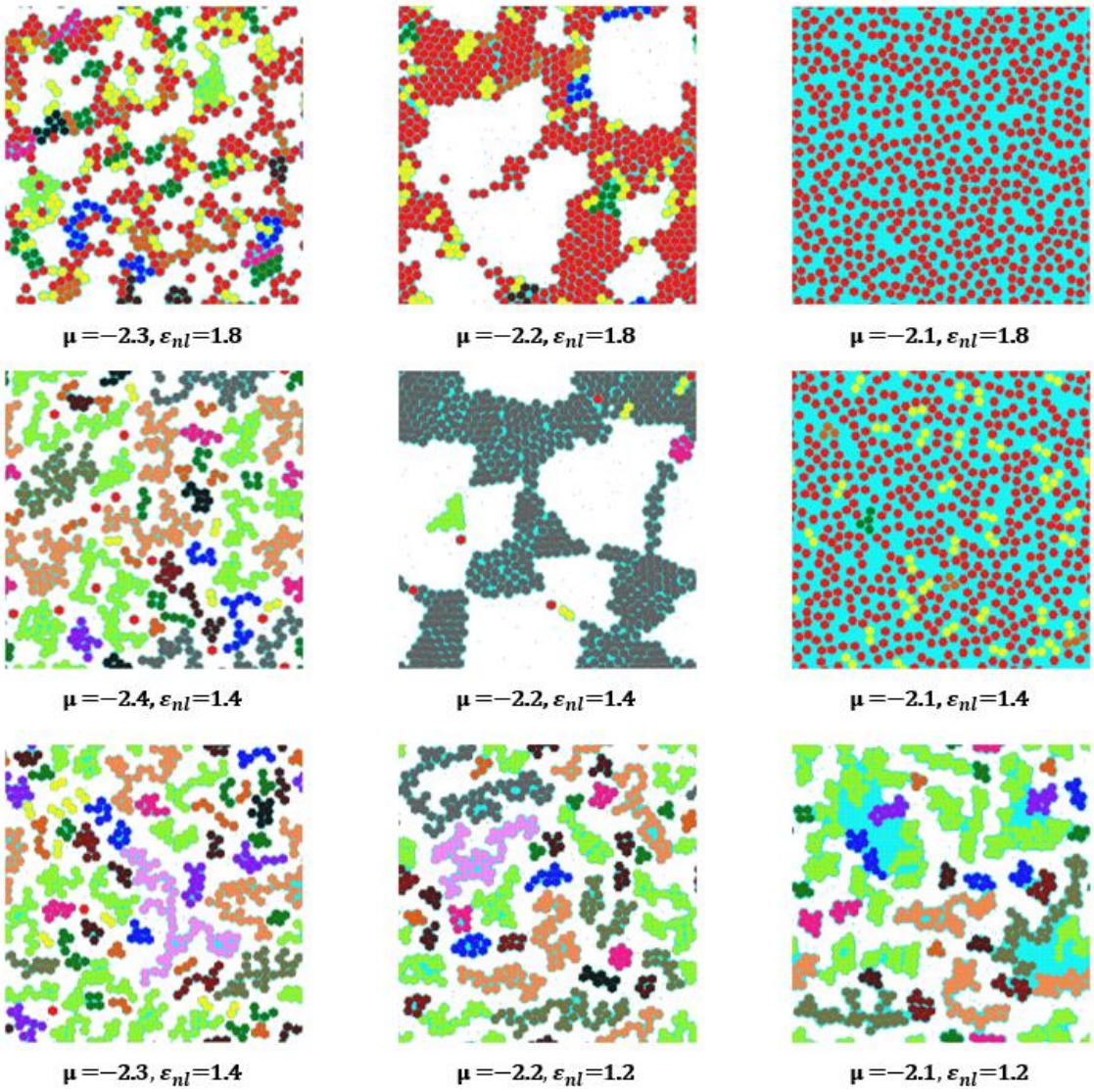

Figure 26: Microstructures for different chemical potentials (μ) and interaction energies (ε_{nl})

This can be understood by observing the difference in the contact area ratio for $\mu = -2.1$ and other. In other cases, due to the less amount of time for diffusion of particles, we can observe that there is less difference in the contact area ratio but still we

can observe that the nature of the curves is decreasing which shows that the effect of diffusion has started from $\varepsilon_{nl} = 1.2$.

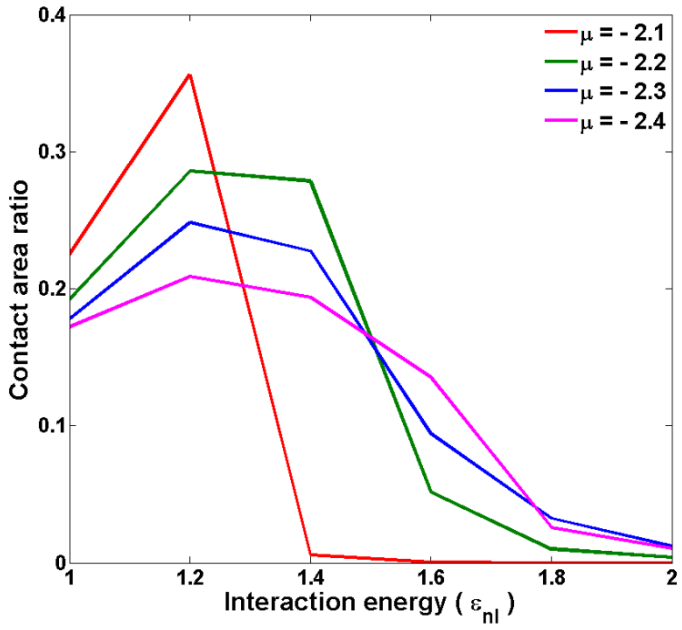

Figure 27: Variation of contact area ratio with respect to interaction energy and chemical potential

The final microstructure in Figure 28 give a very clean idea of the above discussion. Though the average cluster size is highest, for the left side top figure we can clearly see the solvent is in between the particles which reduce the area of contact between particles. And the right bottom figure gives us an idea that due to the dispersion of particles the area of contact has decreased and also it shows that the diffusion has taken over the binding strength of the particles. Previously it is discussed that if the evaporation rate is moderate and the interaction energy ε_{nl} is higher than ε_{nn} then the process is said to be an evaporative induced process. In this process we can clearly observe that the particles are pushed by the increasing gas front. In the Figure 28 left bottom microstructure, most of

the particles are single particles surrounded by the solvent and most of the particles are close enough to form a cluster. But as the ε_{nl} value increases the diffusion of the particles increases which results in such close packed nanoparticles due to the push of increasing gas front. If the evaporation rate is high then the diffusion of the particles will be over taken by the increasing gas front. So the resulting microstructure will not be as closed packed as moderate evaporation rate.

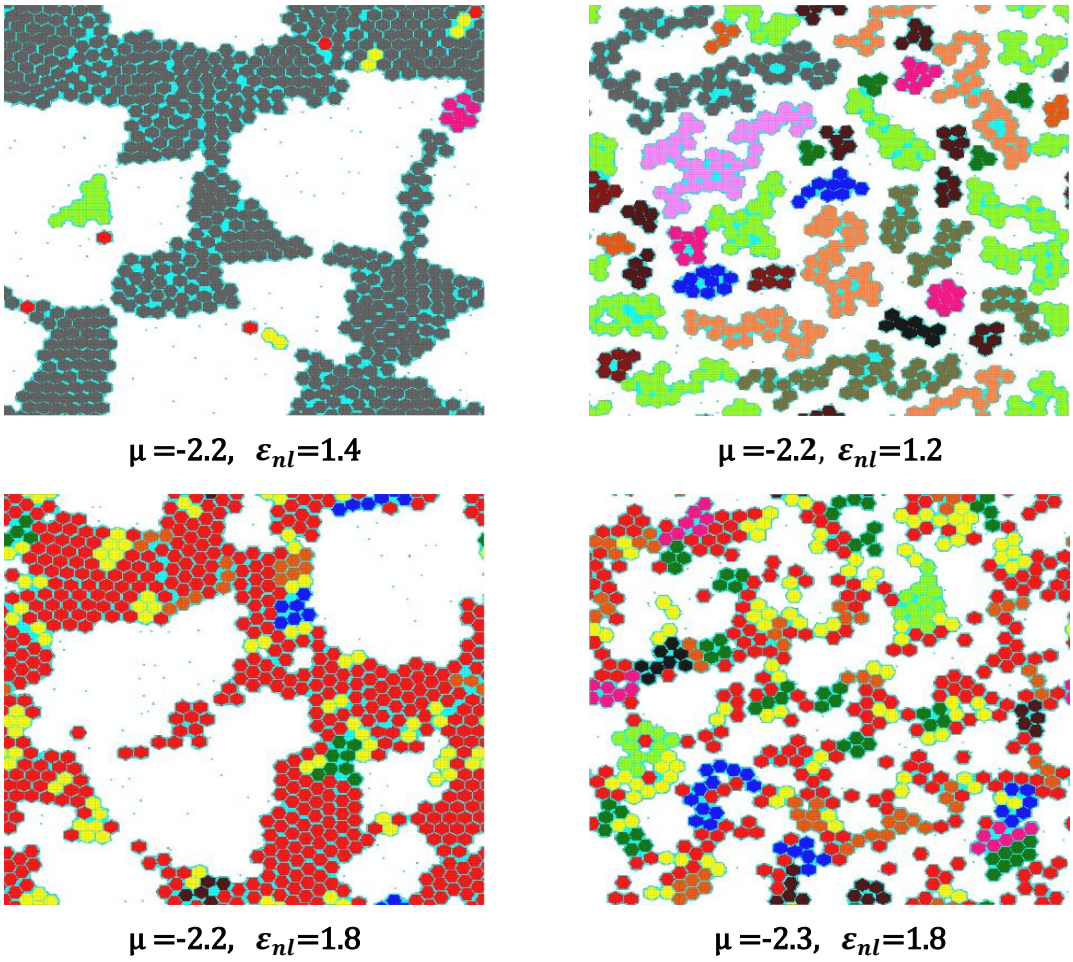

Figure 28: Microstructure at different points in the contact area curve

CHAPTER V

DEPOSITION OF HEXAGONAL NANOPARTICLES AND BINDERS ON THE SUBSTRATE

From the previous chapter, we can understand how different physicochemical factors affect the aggregation of nanoparticles. And how each nanoparticle interacts with other particles in a drying environment. In this chapter, we will introduce the soft binders into the system and discuss how these particles affect the deposition of the active material on the substrate. The study also investigates on the effect of different physicochemical factors on the surface roughness of the film and the distribution of binders in the film formed.

Similar to the previous model we have considered a coarse-grained lattice gas model of size 250X 250 and the deposition of the hexagonal nanoparticles during the evaporation of the solvent is studied. In this model, rotation and translations of the nanoparticles are also considered. The dynamics of the system includes the diffusion of binders and hexagonal nanoparticles, rotation of the active particles and evaporation of the solvent along the thickness of the film. During the processing of an electrode, the slurry is spread on the substrate and dried in the oven. During the drying, evaporation of the solvent proceeds from the top and slowly all the particles present in the solvent will deposit on the substrate.

In this model particles can diffuse in all the four directions but since the evaporation is happening from the top edge of the domain effective diffusion of the particles will be along the thickness of the film. Periodic boundary conditions are

incorporated on both sides of the domain to include the continuity effect. Since at nanoscale, local condensation of the gas phase can also happen at the interface along with the evaporation of the solvent. So the top most layer of cells at the interface are considered along the length of the substrate and checked for the evaporation and the condensation.

Soft binders are the particles used to bind the nanoparticles to the substrate and the other components of the electrode. They are the soft polymeric materials which are highly elastic in nature. Initially, binders are generated as straight tubular-like structures randomly placed in the domain. But since the binders are well mixed in the slurry their shape will be distorted. So in order to attain that distorted shape binders are relaxed for a while before the dynamics of the system is started. Diffusion of the binders can happen from either of the sides (head or tail). So randomly, one of them is chosen as the head cell its diffusion into the surrounding the possible three cells is checked. The Hamilton is calculated on the local structure of the binder and probability of transition is calculated. If it is greater than the random number, diffusion of the cell is accepted. Once the head cell diffuses into the solvent rest of the binder cells will occupy the position of the preceding cells of the binder.

The microstructure of the system can be explained by the following Figure 29, which gives an idea of how each particle in the system is before the start of the MC process. From the above discussion, it can be clearly seen that binders exhibit some complex structures. And the nanoparticles are rigid and exhibit random orientation. The evaporating gas front will move down as the solvent evaporates.

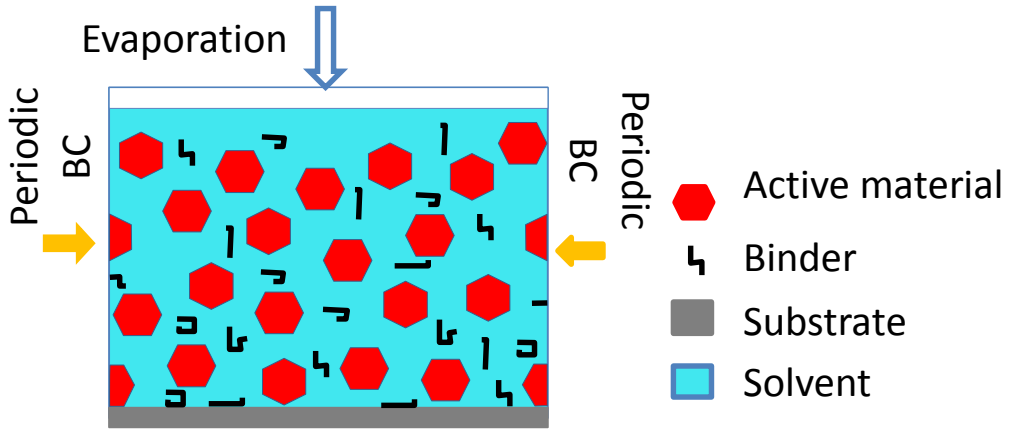

Figure 29: Elucidation of the model

In this particular task, our main goal is to find the effect of binder on the system. During the evaporative induced process, the dynamics of the system is mainly affected by the interaction energies between two species, chemical potential, and temperature. Some of the minor factors which affect the system are the number of particles, and size of the particles. Since we are particular to find the effect of binders on the system following factors are considered in our study

1. Chemical potential: Chemical potential is the driving force for the evaporation process. The presence of the soft polymers decreases the chemical potential due to the difference in the interaction between the different species in the system.
2. Temperature: The temperature of the system is controlled by the (k*T) value. From the probability of state transition, as the temperature increases the chances for the diffusion of the particles and evaporation of the solvent increases. So the distribution of the binders and their diffusion is effected by varying the temperature.

3. Interaction energies: Interaction energy between two species affects the diffusion of the particles. Since there are different types of species/particles present in the system, only the strong interaction energies which can affect the film formation are considered in our study. In this model, the interaction energy between the nanoparticles and binders is a most important factor which decides the distribution of binders. And interaction energy of the particles with the solvent decides their diffusions in the solvent. The other weak interaction energies are considered to be constant.

From this it can be understood that the strong factors we are considering for the study are

- Interaction energy between nanoparticle and the solvent
- Interaction energy between binder and the solvent
- Interaction energy between nanoparticle and binder
- Chemical Potential
- Temperature
- Binder length

Initially, the particles (Nanoparticles and Binders) are distributed in the solvent randomly. During the evaporation, all the particles in the system will be exhibiting a random motion inside the solvent. Evolution of the microstructure is explained through Figure 30.

During the evolution of the microstructure, the total energy of the system and the average film thickness decreases with respect to time. When the decrease in the slope of

the total energy curve decreases less than 10^{-7}, the equilibrium state of the system is said to be reached. Figure 31 gives an idea of the two stages during the evolution of microstructure. In the first stage, the particles are positioned randomly across the domain and the state of energy is high. As the time passes, the particles will spontaneously diffuse into the solvent in order to get the lower energy state which is more stable. After a while, the particles self-assemble among themselves and meta-stable state of the system is reached. In the first stage, the change in total energy is not only due to the diffusion of particles but also due to the evaporation happening in the system.

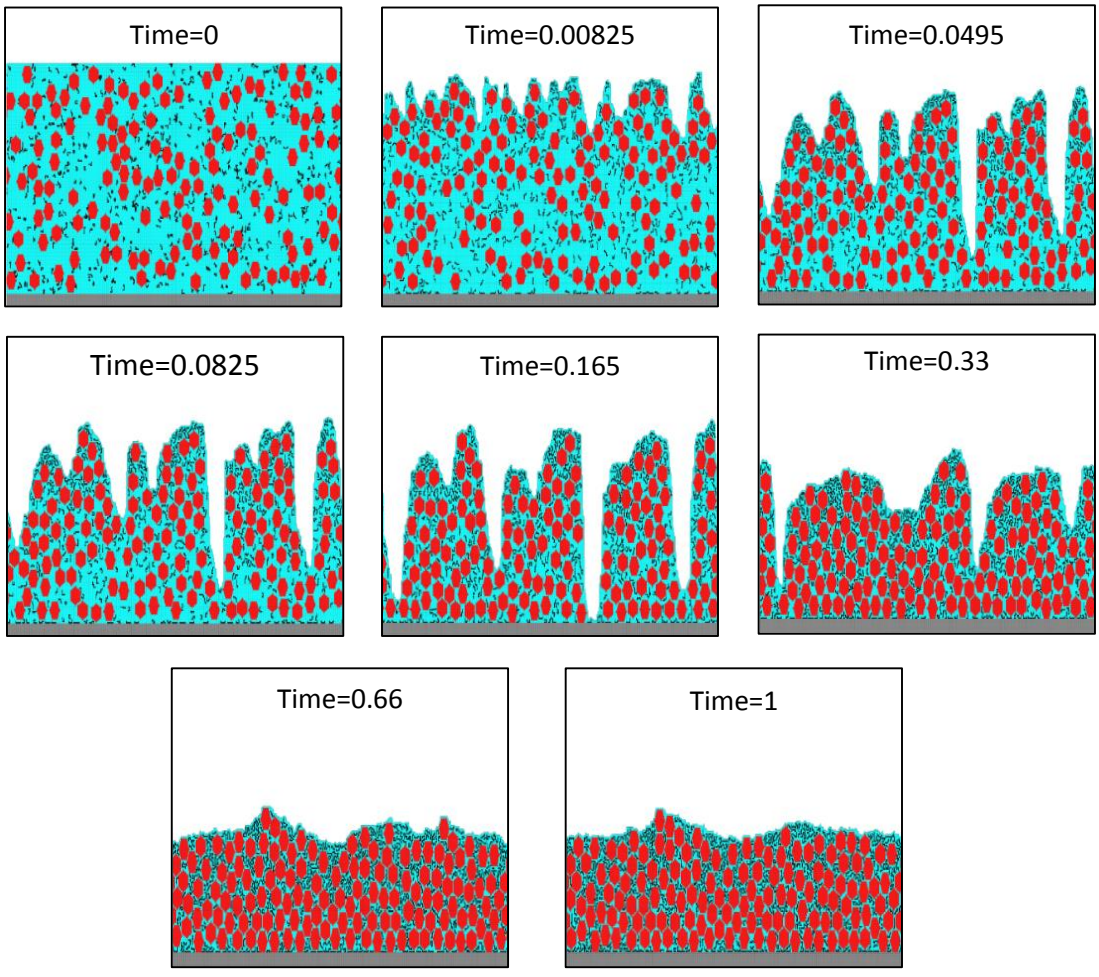

Figure 30: Evolution of the microstructure

In the second stage of the drying process, a further decrease in the energy can be observed due to the evaporation of the solvent. We can also observe that the particles will exhibit a random walk in the lattice. As the evaporation proceeds the solvent present in the system decreases by which the attained meta-stable gets disturbed. So the particles will again try to diffuse into the solvent to attain an equilibrium state.

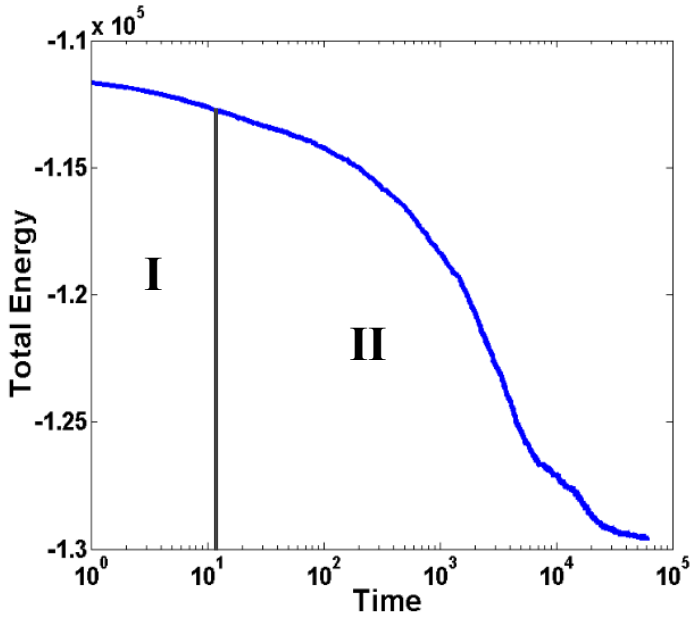

Figure 31: Evolution of total energy of the system

From the figure we can understand that the equilibrium state cannot be reached unless, the rate of evaporation and condensation becomes almost equal. By the end of the second stage the particles will reach an equilibrium state and the final microstructure can be obtained. But in the final microstructure, we can still observe little solvent present in the system. Through this model, complete evaporation of the solvent can be attained at higher evaporation rates and temperatures only. Similar to total energy, the normalized average thickness also decreases with time. After a while, the thickness of the system

remains almost same, and the nanoparticles position will not be changing much. But, the binders will exhibit the walk in the solvent present between the nanoparticles.

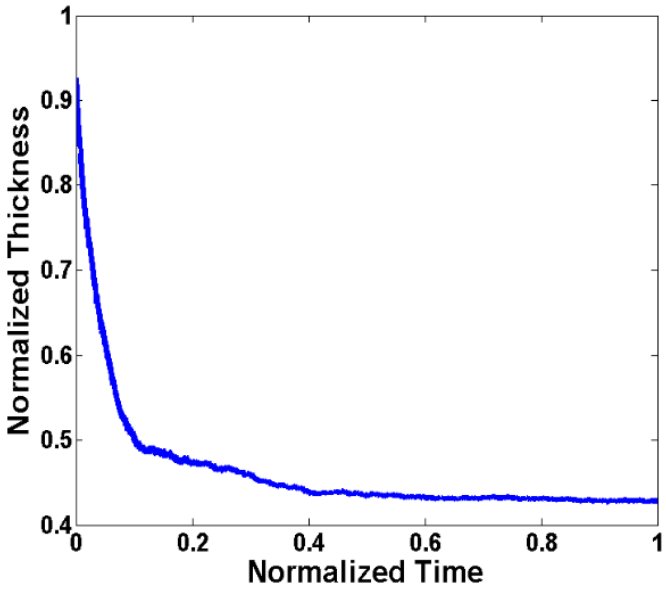

Figure 32: Evolution of average film thickness

Effect of strong parameters

Interaction energies between particles and the solvent

As explained above we can understand that the interaction energy between the particles and solvent will influence the diffusion of the particles in the solvent. With different interaction energies, we can obtain different final microstructures. Figure 33 shows final microstructures obtained at different interaction energies.

We can observe that the texture of the surface varies from one microstructure to the other. If the interaction energy between the particles and the solvent is high, then the particle tries to diffuse into the solvent thereby creating low texture quality. If the

interaction energy between the binder and the solvent is not very high then they will not diffuse into the solvent thereby we can attain a good texture quality. If the interaction energy between the active particles and the solvent is high, the active particles will diffuse in the little solvent present in the solvent thereby attaining a compact film with good texture quality.

As it can be seen we get lowest surface roughness for $\varepsilon_{nl} = 2.4, \varepsilon_{bl} = 2.0$ case and maximum surface roughness is for $\varepsilon_{nl} = 2.4, \varepsilon_{bl} = 2.4$ case. As explained above, for a good texture quality we need lower ε_{bl} than compared to ε_{nl} values. If we can get a structure with very few binders on top of the film, then we can attain a film with good surface texture.

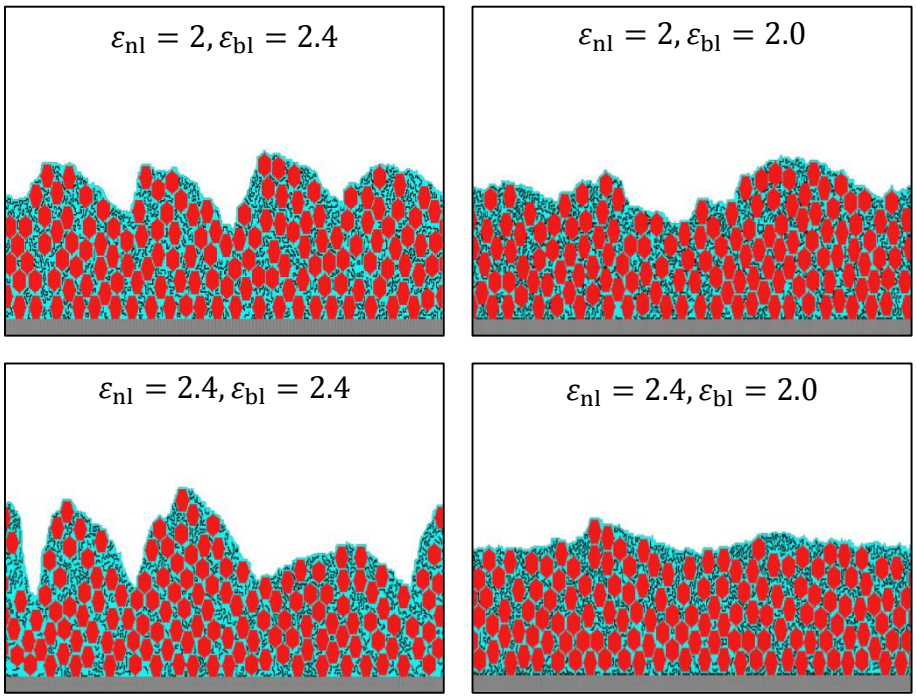

Figure 33: Final microstructure for different interaction energies of particles with solvent

Effect of binder length

The diffusion of the active particles decreases as the length of the binder increases. But since the volume fraction of the binder is constant, the number of particles decreases which allows the particles diffuse faster. And also, since the number of solvent cells available at the top increases the evaporation front will also move faster. Thereby creating the finger like structures on the substrate.

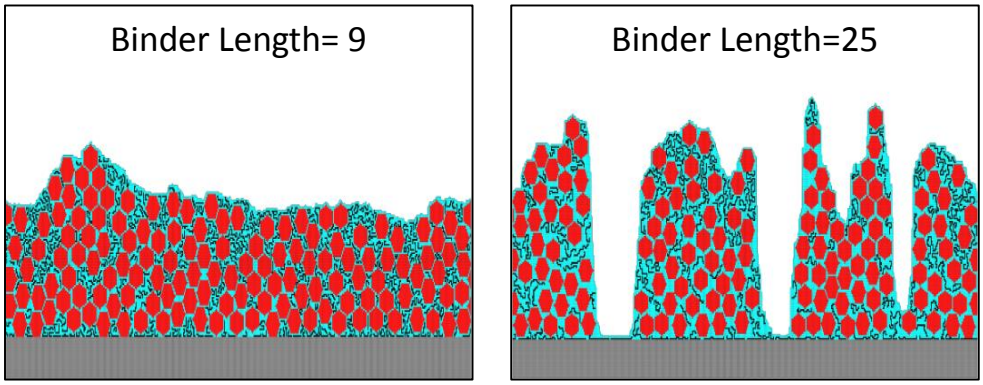

Figure 34: Microstructures of the film for different binder lengths

Effect of very strong factors

In this section, the effect of very strong parameters on various factors like average film thickness, total energy, binder's distribution, the volume fraction of each species and the surface roughness are investigated. Each of the factors is discussed in detail to understand their effect on the film morphology and particles distribution.

Average film thickness and surface roughness

Average film thickness gives an idea of the compactness of the film formed. It also gives an idea of the rate of decrease of the film thickness. From the Figure 35 & 37, we can observe the effect of chemical potential on the rate of decrease of the film thickness.

Evaporation rate increases as the chemical potential decreases, due to the fast growing gas front particles will experience less time for diffusion. Hence, the film formed will not be uniform due to the unavailability of the solvent required for dispersion of particles. Hence the average film thickness increases due to the finger like structures. Whereas at lower evaporation rates the particles will get enough time to settle down on the substrate. This can be observed through the final microstructures shown in Figure 35. So surface roughness and average film thickness increase with the chemical potential.

Since the evaporation rate also depends on the temperature, as the temperature increases we can observe that the diffusion of the particles also increases. So at higher temperatures we can observe that the film formed is more uniform though the evaporation rate is also high at higher temperatures. Figure 35 gives you an idea of how the temperature is affecting the microstructure. At lower temperatures we can observe that both evaporation rate and diffusion are low. Due to which particles will get enough time to diffuse. Since the diffusion of binders is slower than active particles, we can observe that binders are obstructing the gas front. So as the temperature increases, first the increment in the evaporation rate increases as it is more sensitive towards the change in temperatures. As the temperature increases, diffusivity takes over the evaporation rate leading to the uniform film. Similarly, the average thickness of the film will be low at higher temperatures. And the thickness increases at moderate temperatures and will decrease at lower temperatures.

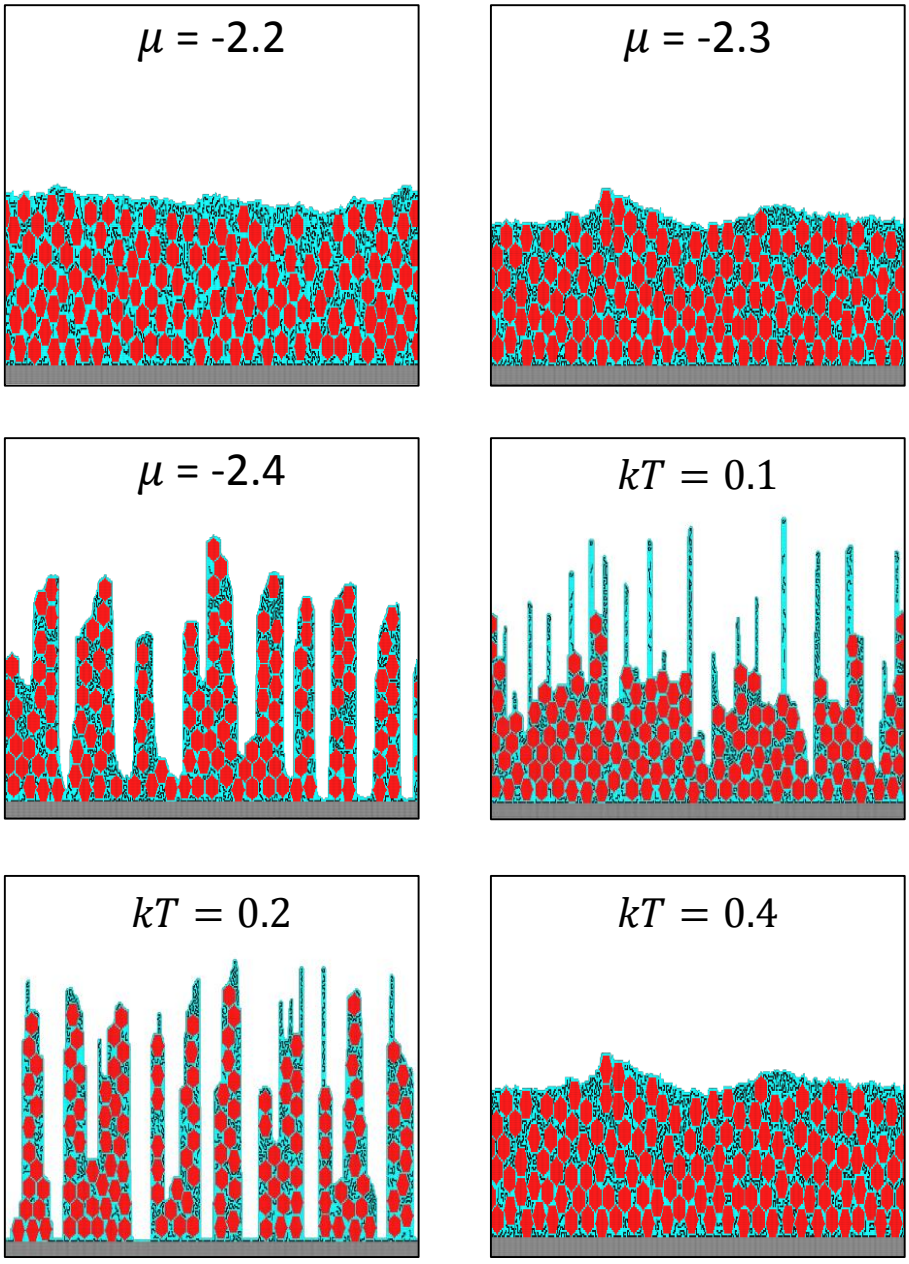

Figure 35: Final microstructures at different chemical potentials and temperatures

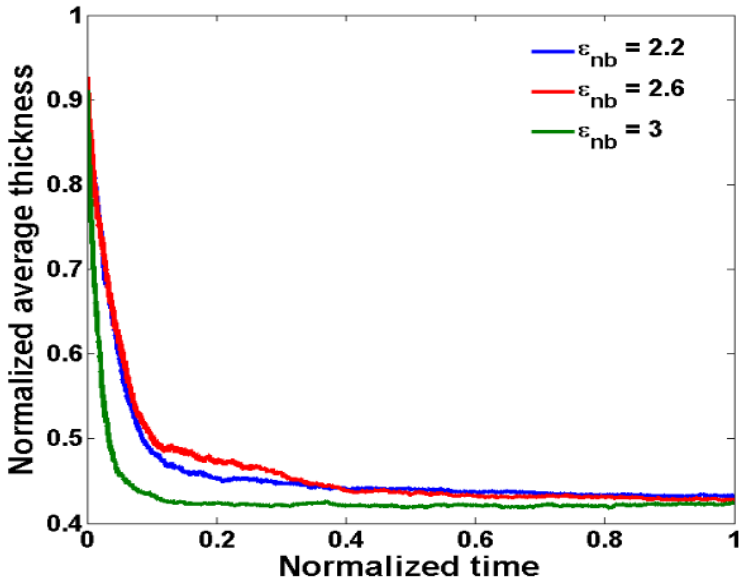

Figure 36: Effect of interaction energy on average film thickness

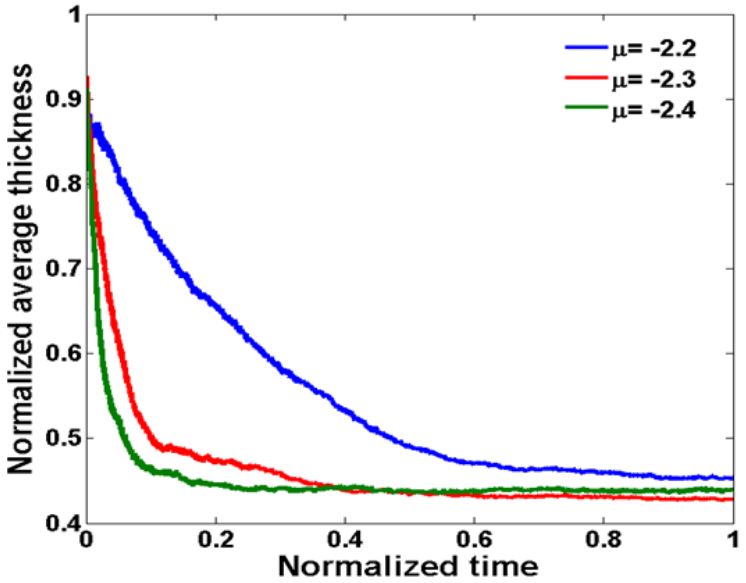

Figure 37: Effect of chemical potential on the average cluster size

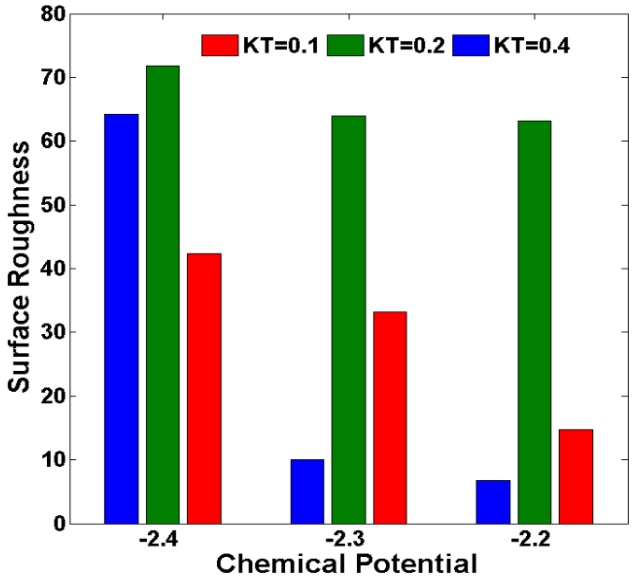

Figure 38: Effect of temperature and chemical potential on surface roughness

The surface roughness of the film is calculated to show the texture quality of the film formed on the substrate. If the surface film formed is uniform then the surface area of the electrode exposed to electrolyte would be low. Whereas if the film formed is not uniform then the surface area exposed to the electrolyte will be more. Which is good for driving more charge from the electrode.

The surface roughness is calculated by finding the standard deviation of the film thickness along the length of the film. Chemical potential and temperature affect the surface roughness to a greater extent than compared to the interaction energy between the nanoparticles. The above discussion gives us an idea of surface roughness variation with chemical potential and temperature.

Interaction energy between active particles and the binders play an important role in the distribution of binders. From Figure 36 it is clear that interaction energies between active particles and the binders don't play a big role in average cluster size.

Total energy

The total energy of the system directly depends on chemical potential, interaction energies but not on temperature. From the energy equation shown before, it doesn't contain any temperature term. But the rate of energy variation does depend on the temperature. Since the diffusion of the particles and evaporation of the solvent directly affect the total energy of the system. From Figure 40 we can understand that total energy increases with respect to decreasing chemical potential. And with respect to time, the energy difference decrease as the number of solvent cells decreases.

At lower chemical potentials evaporation rate will be high. So the rate at which energy curve decreases is more for lower chemical potentials compared to others. From Figure 39 it can also be noted that for all the temperature values the initial total energy is same. But when the system reaches equilibrium energies decrease with respect to the temperature. This is because of the effect of temperature on diffusion and evaporation.

From Figure 41 we can observe that the energy difference between different cases is zero initially as the particles are randomly placed in the lattice. But as the evaporation proceeds, the particles will come closer and hence, there is a little difference in the total energy due to the difference in the interactions between the particles. The rate of decrease of the total energy depends on the diffusion of particles and the evaporation of the solvent, which depends on the random number generated. So it varies randomly.

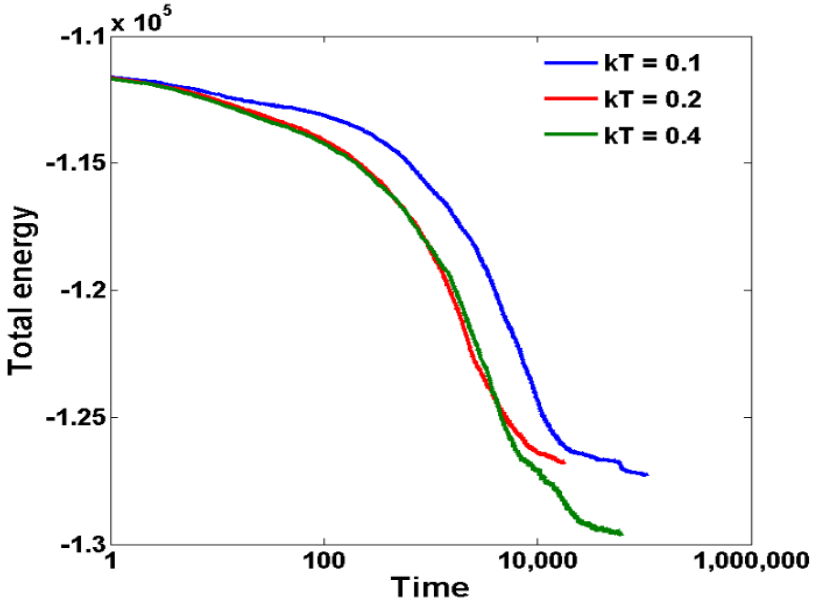

Figure 39: Effect of temperature on the total energy

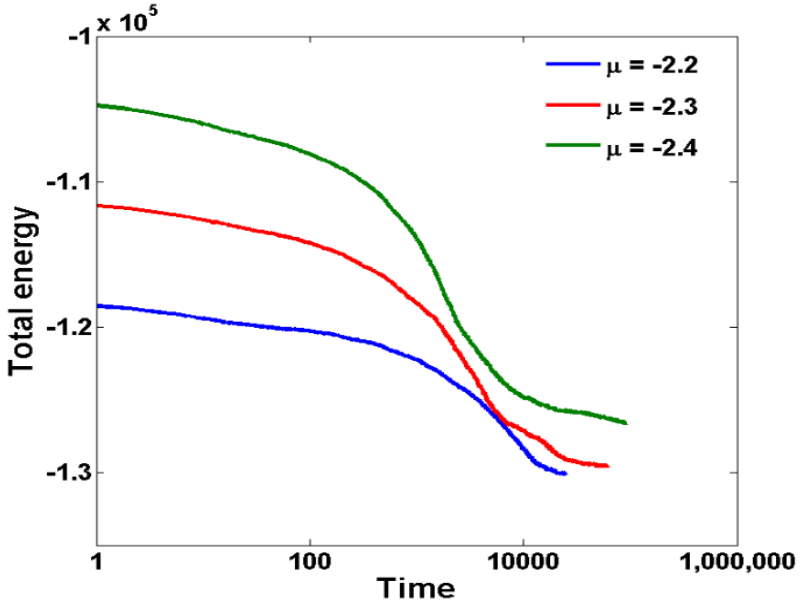

Figure 40: Effect of chemical potential on the total energy

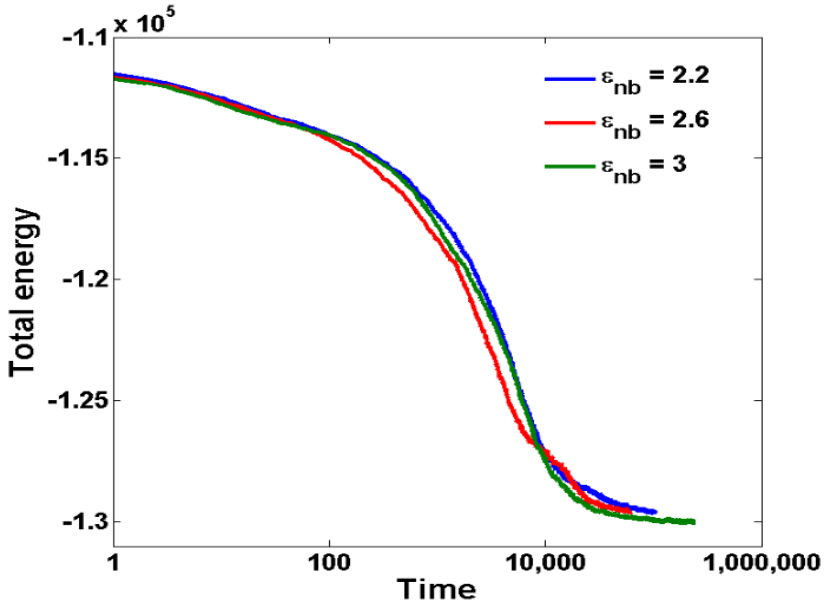

Figure 41: Effect of interaction energy on total energy

Volume fraction

The volume fraction of the solvent depends on both chemical potential, and temperature. Since the evaporation dynamics is affected by these parameters. It is clear that as the chemical potential decreases the evaporation rate increases. So the rate of change of volume fraction of the solvent cells will be higher at lower chemical potentials. So eventually, the volume fraction of the nanoparticles also increases at a higher rate with respect to the decrease in chemical potential. Figure 42, 43 shows the effect of chemical potential and Figure 44, 45 shows the effect of temperature on volume fraction of solvent and active particles. Similarly at higher temperatures also, we can observe that the evaporation rate is high. So as the temperature increases the rate of decrease in solvent volume fraction increases. We can also observe that at $kT = 0.2$, the

rate of decrease in the volume fraction of solvent is almost close to $kT = 0.4$. This shows that the evaporation rate in the case of $kT = 0.2$.

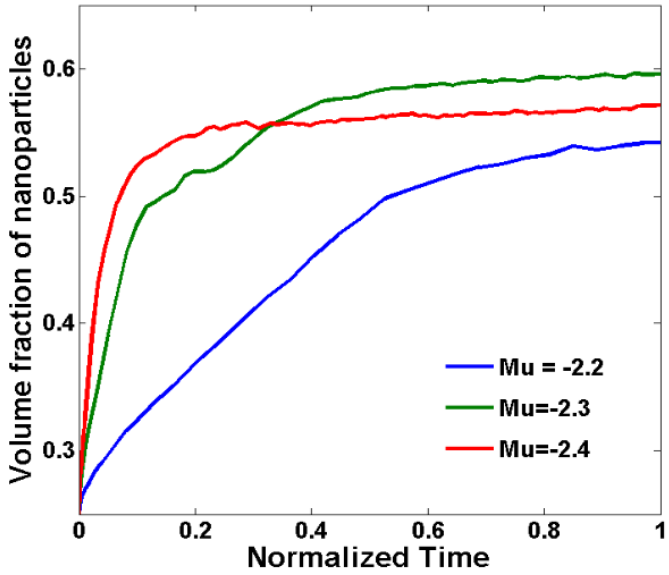

Figure 42: Effect of chemical potential on volume fraction of the nanoparticles

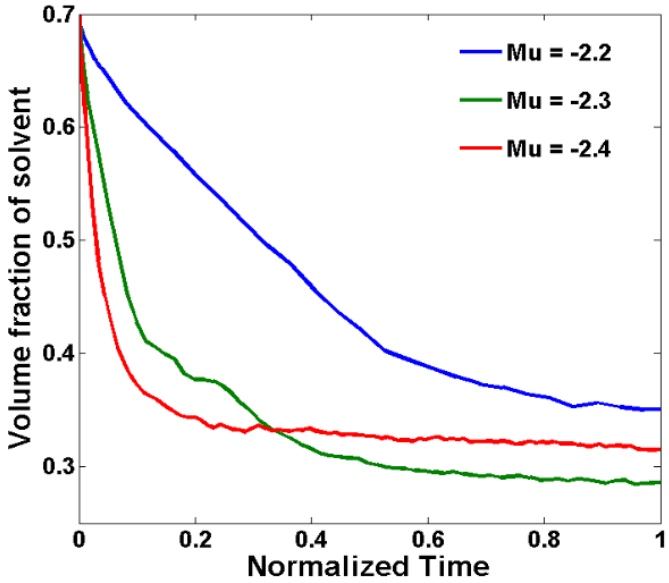

Figure 43: Effect of chemical potential on volume fraction of solvent

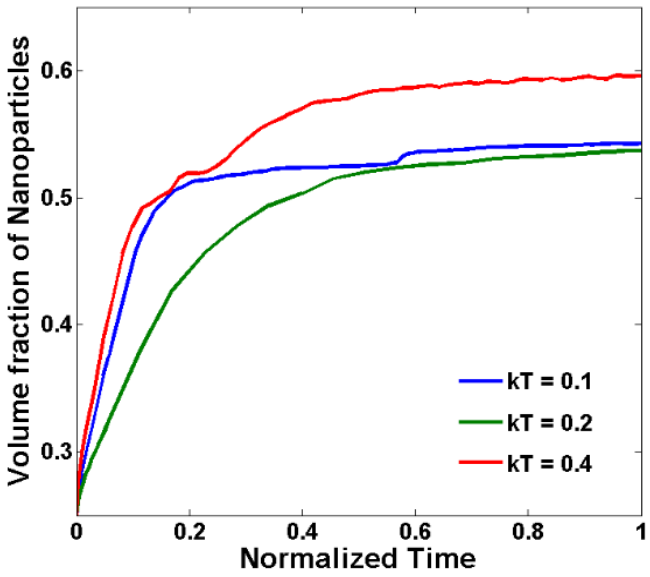

Figure 44: Effect of temperature on the volume fraction of the active particles

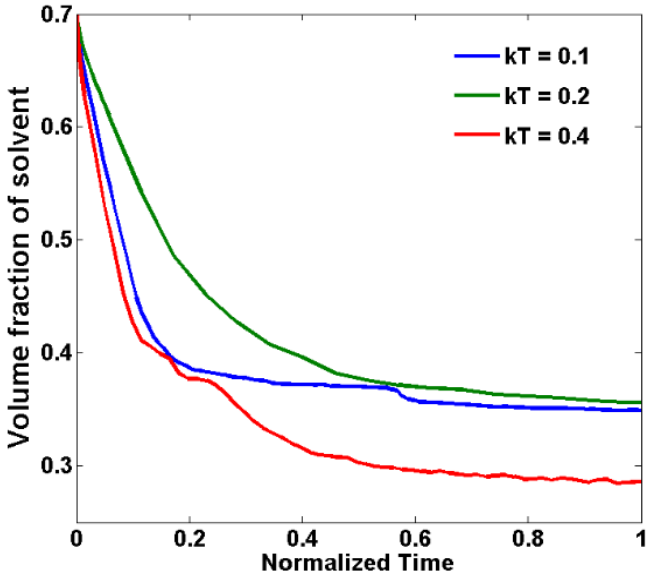

Figure 45: Effect of temperature on the volume fraction of the solvent

Distribution of binders

Distribution of binders is one of the most important features of the electrode microstructure which is going to affect the performance of the battery. Previous studies have explained that the most of the binders accumulate at the top of the film been formed, which is not good for the electrode as it reduces the interactions of the nanoparticles with the electrolyte and reduces the chemical reactions important for the production of Li ions. Similarly, if the distribution of binders is more at the surface of the substrate, the electrons reached to the current collector will not be utilized to form the Li in the electrode. Due to which the electrochemical reactions stops, and the production of Li ions doesn't take place.

One of main motivation for this study is to find out a way to control the distribution of binders. The volume fraction of binders and coordination number are used to understand binders distribution in the film formed. Coordination number is the physical quantity which resembles the number of binders present in the vicinity of a nanoparticle. It is calculated by considering a circle of radius R_CN around the nanoparticle and plotting the number of binders surrounding the nanoparticle.

Effect of interaction energy

Interaction energy between the nanoparticles and the binders is similar to the interaction energy between the nanoparticles. If this interaction energy increases then the dispersion of the particles decreases, thereby forming the clusters. At higher interaction energies due to the higher interaction between the different species, each active particle will be surrounded by the binders. From the Figure 46 and Figure 47, it is clear that the

concentration of the binders shifts down as the interaction energy increases. We can also observe that the distribution of binders is also becoming uniform with the increase in the interaction energy.

Effect of chemical potential

Chemical potential has a very big effect on the film formation. As the chemical potential increases the rate of evaporation increases which forces the particles towards the surface of the substrate. Therefore, the diffusion time for the particles will be low. From Figure 47 and Figure 48, it can be seen that at lower chemical potentials the distribution of particles is happening relatively better. If the interaction energy between the active particles and binders is not very high, then the binders at the surface of the film will try to diffuse up thereby forming a film with a higher volume fraction of binders on top of the film. Whereas, at high temperatures due to fast evaporation of solvent finger-like structures are formed over the substrate. Because of which the distribution of binders is not uniform. From the coordination number contour map, we can observe a better distribution of binders in the case of moderate chemical potential due to the push created by the gas front on the particles. If the chemical potential decreases to a very low value, then fingered like structures are formed.

Effect of temperature

Figure 49 & 50gives us the information on the distribution of binder with respect to temperature. At higher temperatures we can observe that the diffusion of the particles will be more thereby creating a uniform distribution of particles. If the temperature is low, the evaporation dynamics takes over the diffusion of particles thereby creating the

non-uniform distribution of particles. At $kT = 0.1$ due to lower diffusion of binders, spikes with binders at top observed. Figure 49 also gives us the same idea.

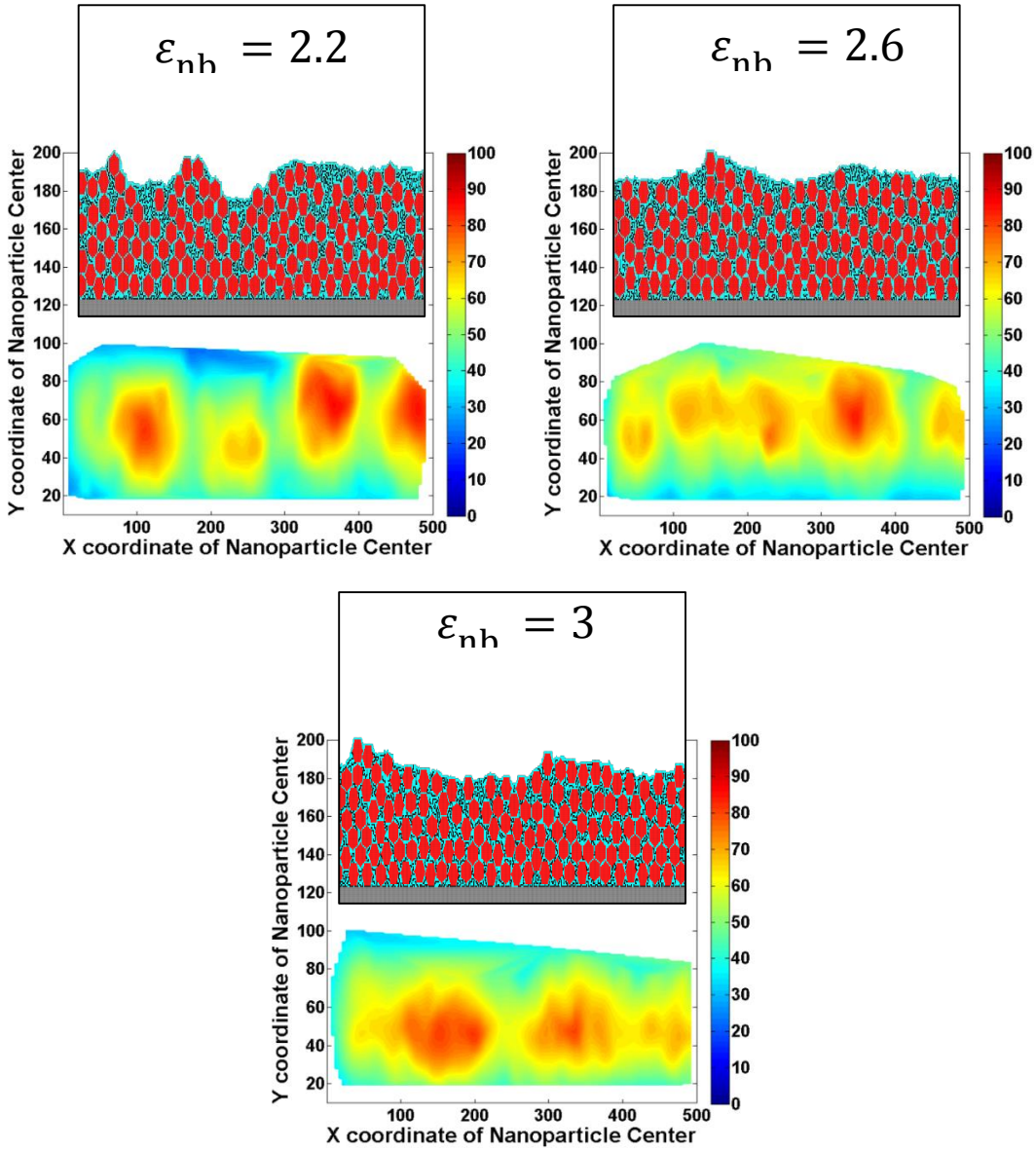

Figure 46: Effect of interaction energy on coordination number of binders

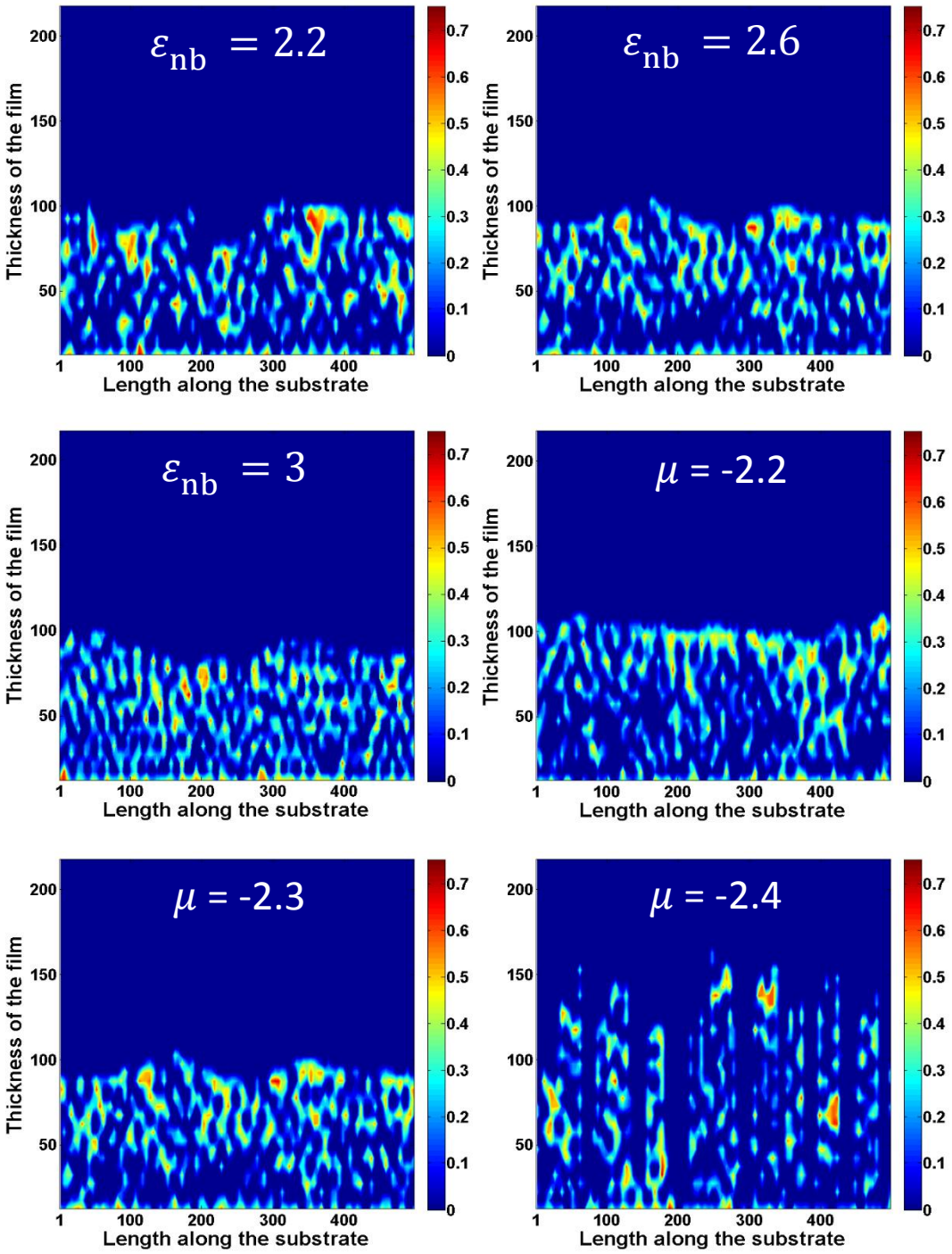

Figure 47: Effect of interaction energy and chemical potential on volume fraction of binders

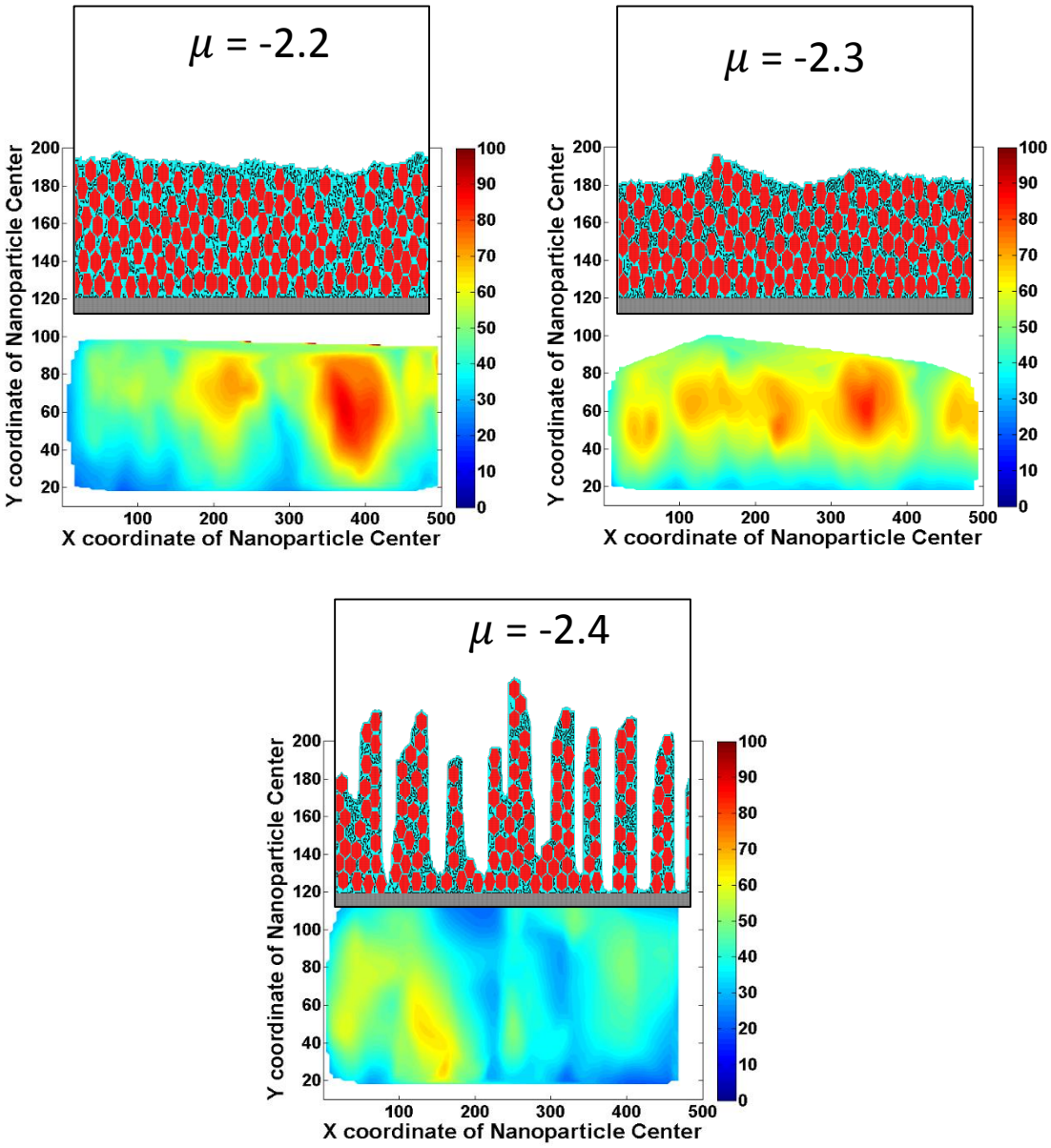

Figure 48: Effect of chemical potential on the coordination number of binders

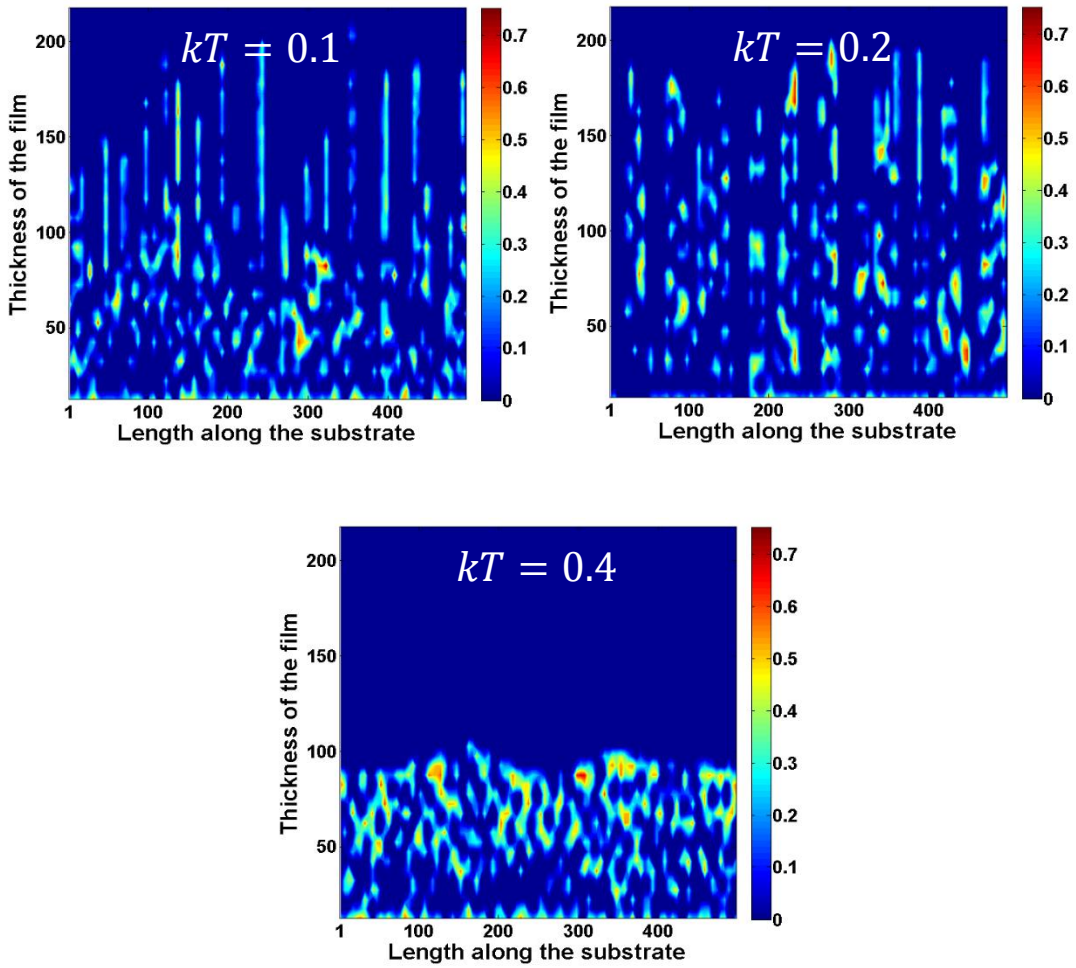

Figure 49: Effect of temperature on volume fraction of binders

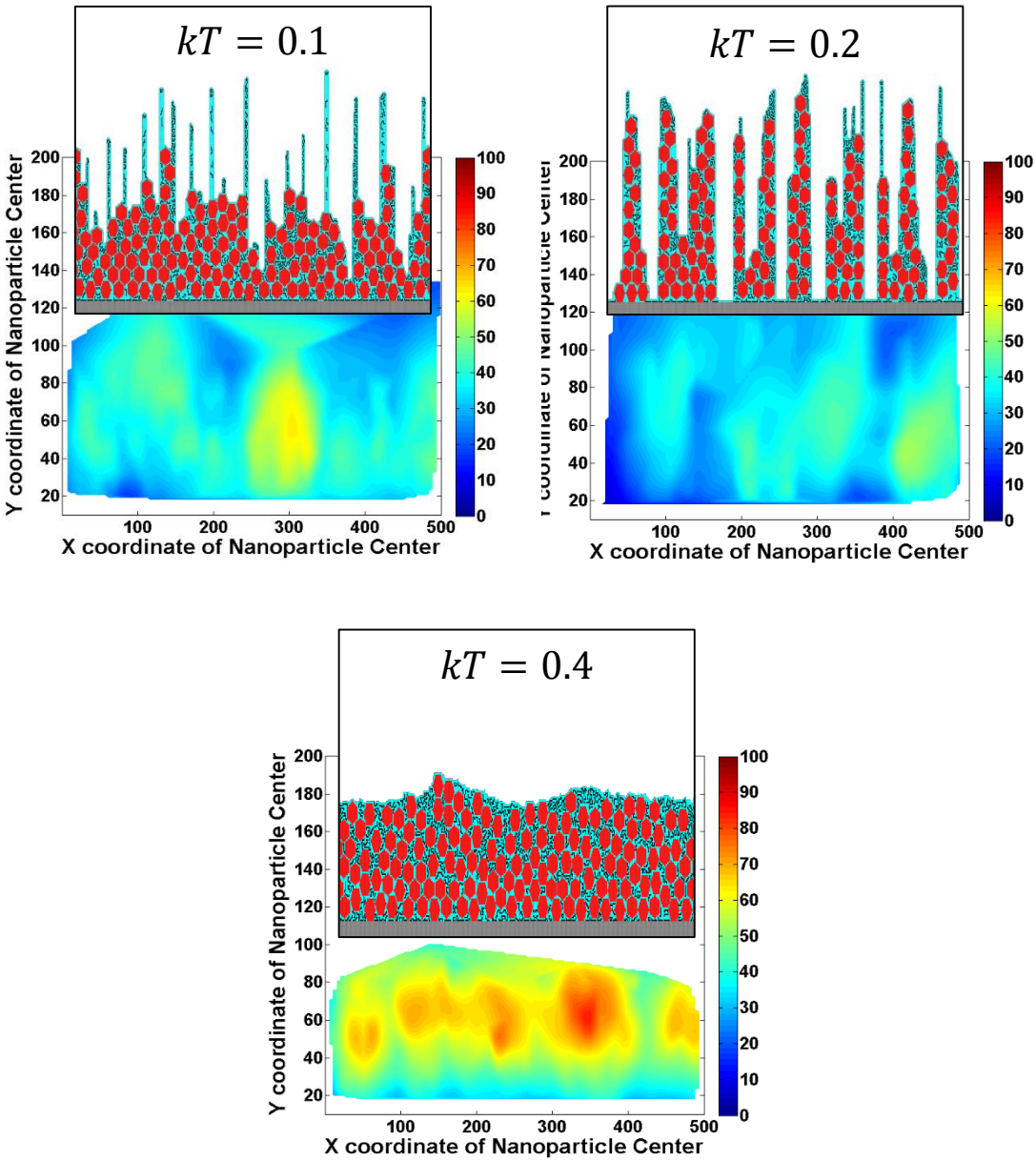

Figure 50: Effect of temperature on the coordination number of binders

CHAPTER VI

CONCLUSIONS AND FUTURE WORK

In this study, I would like to address the issue of how electrode microstructures are formed at various physicochemical conditions and how can they be controlled. In the analysis, I have focused on the stratification model which is a continuum model and the mesoscale model.

Through the continuum model, the variation of volume fraction along the thickness of the film being formed and the effect of Peclet number, Sedimentation number and Initial volume fraction of secondary particles on the distribution of active particles is discussed. It is found that volume fraction of the active particles increases with respect to time as the solvent evaporates and their distribution along the height of the film depends on Peclet number and Sedimentation number. If the Peclet number is high, due to the high evaporation rate we can observe that maximum volume fraction of the particles is reached at the top layer. If the sedimentation number is high the particles sediment quickly thereby, increasing the volume fraction at the bottom surface (i.e. substrate). If the volume fraction of the secondary particles is increased, the viscosity of the slurry increases due to which the diffusion and sedimentation of the particles will be hindered.

The distribution of the secondary particles in between the secondary particles is studied for certain cases. The effect of temperature and chemical potential on the deposition of these secondary particles on the active particle surface is shown. If the temperature of the system increases diffusion of these secondary particles increases, due

to which a uniform film can be formed over the surface. If the chemical potential increases the evaporation rate increases due to which columnar finger-like structures are formed.

Considering the ongoing research on the usage of nano-sized active particles for the electrodes, I have modelled hexagonal active particle and snake-like structure binder's assembly by using KMC method. This study focuses on the factors which affect the aggregation of particles and their distribution in the film formed. I found that increasing the temperature of the system increases the diffusion of particles and thus uniformity of the film increases. With the increase in the chemical potential, as the evaporation rate increases. Thereby columnar finger-like structures are formed. With the increase in interaction energy between the active particles and binders, the distribution of the binders can be controlled. At higher interaction energies, binders can be locked in between the active particles and the film formed is also more homogeneous.

Coupling the effect of nanoparticle assembly with the stratification model can help in analyzing the distribution and arrangement of all the electrode constituents and can prove an interesting extension of the current study. Future work can also concentrate on developing a continuum model taking into consideration the distribution of nanoparticles. The formation of thin film electrodes with the active particles, binders, and the conductive additives can give us a good understanding on the distribution of each particle during the drying process and the factors effecting them.

REFERENCES

1. Tarascon, J.M. and M. Armand, *Issues and challenges facing rechargeable lithium batteries.* Nature, 2001. **414**(6861): p. 359-367.
2. Tarascon, J.M., *Key challenges in future Li-battery research.* Philosophical Transactions of the Royal Society a-Mathematical Physical and Engineering Sciences, 2010. **368**(1923): p. 3227-3241.
3. Armand, M. and J.M. Tarascon, *Building better batteries.* Nature, 2008. **451**(7179): p. 652-657.
4. Etacheri, V., et al., *Challenges in the development of advanced Li-ion batteries: a review.* Energy & Environmental Science, 2011. **4**(9): p. 3243-3262.
5. Arico, A.S., et al., *Nanostructured materials for advanced energy conversion and storage devices.* Nature Materials, 2005. **4**(5): p. 366-377.
6. Bruce, P.G., B. Scrosati, and J.M. Tarascon, *Nanomaterials for rechargeable lithium batteries.* Angewandte Chemie International Edition, 2008. **47**(16): p. 2930-2946.
7. Daniel, C., *Materials and processing for lithium-ion batteries.* Jom, 2008. **60**(9): p. 43-48.
8. Li, J., C. Daniel, and D.L. Wood, *Cathode Manufacturing for Lithium-Ion Batteries.* Handbook of Battery Materials, Second Edition, 2011: p. 939-960.

9. Manthiram, A., *Materials Challenges and Opportunities of Lithium Ion Batteries (vol 2, pg 176, 2011).* Journal of Physical Chemistry Letters, 2011. **2**(5): p. 373-373.

10. Manthiram, A., et al., *Nanostructured electrode materials for electrochemical energy storage and conversion.* Energy & Environmental Science, 2008. **1**(6): p. 621-638.

11. Barai, P. and P.P. Mukherjee, *Mechano-Electrochemical Model for Acoustic Emission Characterization in Intercalation Electrodes.* Journal of The Electrochemical Society, 2014. **161**(11): p. F3123-F3136.

12. Li, J.L., et al., *Optimization of LiFePO4 Nanoparticle Suspensions with Polyethyleneimine for Aqueous Processing.* Langmuir, 2012. **28**(8): p. 3783-3790.

13. Li, J.L., et al., *Lithium Ion Cell Performance Enhancement Using Aqueous LiFePO4 Cathode Dispersions and Polyethyleneimine Dispersant.* Journal of the Electrochemical Society, 2013. **160**(2): p. A201-A206.

14. Liu, G., et al., *Effects of Various Conductive Additive and Polymeric Binder Contents on the Performance of a Lithium-Ion Composite Cathode.* Journal of the Electrochemical Society, 2008. **155**(12): p. A887-A892.

15. Liu, G., et al., *Optimization of acetylene black conductive additive and PVDF composition for high-power rechargeable lithium-ion cells.* Journal of the Electrochemical Society, 2007. **154**(12): p. A1129-A1134.

16. Liu, G., et al., *Particles and Polymer Binder Interaction: A Controlling Factor in Lithium-Ion Electrode Performance.* Journal of the Electrochemical Society, 2012. **159**(3): p. A214-A221.

17. Zheng, H.H., et al., *Cooperation between Active Material, Polymeric Binder and Conductive Carbon Additive in Lithium Ion Battery Cathode.* Journal of Physical Chemistry C, 2012. **116**(7): p. 4875-4882.

18. Zheng, H.H., et al., *Correlationship between electrode mechanics and long-term cycling performance for graphite anode in lithium ion cells.* Journal of Power Sources, 2012. **217**: p. 530-537.

19. Vu, A., Y.Q. Qian, and A. Stein, *Porous Electrode Materials for Lithium-Ion Batteries - How to Prepare Them and What Makes Them Special.* Advanced Energy Materials, 2012. **2**(9): p. 1056-1085.

20. Wang, B., et al., *The synergy effect on Li storage of LiFePO 4 with activated carbon modifications.* RSC Advances, 2013. **3**(43): p. 20024-20033.

21. Zheng, H., et al., *A comprehensive understanding of electrode thickness effects on the electrochemical performances of Li-ion battery cathodes.* Electrochimica Acta, 2012. **71**: p. 258-265.

22. Yang, S., et al., *Morphology-controlled solvothermal synthesis of LiFePO 4 as a cathode material for lithium-ion batteries.* Journal of Materials Chemistry, 2010. **20**(37): p. 8086-8091.

23. Bauer, W. and D. Nötzel, *Rheological properties and stability of NMP based cathode slurries for lithium ion batteries.* Ceramics International, 2014. **40**(3): p. 4591-4598.

24. Kim, K.M., et al., *Effect of mixing sequences on the electrode characteristics of lithium-ion rechargeable batteries.* Journal of Power Sources, 1999. **83**(1-2): p. 108-113.

25. Yang, C., et al., *Performance study of the LiCoO 2/graphite system.* Journal of power sources, 1997. **68**(2): p. 440-442.

26. Rabani, E., *Drying-mediated self-assembly of nanoparticles: A lattice gas model.* Abstracts of Papers of the American Chemical Society, 2005. **229**: p. U656-U656.

27. Rabani, E., et al., *Drying-mediated self-assembly of nanoparticles.* Nature, 2003. **426**(6964): p. 271-274.

28. Rabani, E., *Drying-induced self assembly of nanorods.* Abstracts of Papers of the American Chemical Society, 2010. **240**.

29. Crivoi, A. and F. Duan, *Evaporation-induced formation of fractal-like structures from nanofluids.* Physical Chemistry Chemical Physics, 2012. **14**(4): p. 1449-1454.

30. Crivoi, A. and F. Duan, *Evaporation-Induced Branched Structures from Sessile Nanofluid Droplets.* Journal of Physical Chemistry C, 2013. **117**(15): p. 7835-7843.

31. Crivoi, A. and F. Duan, *Fingering structures inside the coffee-ring pattern.* Colloids and Surfaces a-Physicochemical and Engineering Aspects, 2013. **432**: p. 119-126.

32. Rabani, E. and S.A. Egorov, *Interactions between passivated nanoparticles in solutions: Beyond the continuum model.* Journal of Chemical Physics, 2001. **115**(8): p. 3437-3440.

33. Rabani, E. and S.A. Egorov, *Integral equation theory for the interactions between passivated nanocrystals in supercritical fluids: Solvophobic and solvophilic cases.* Journal of Physical Chemistry B, 2002. **106**(26): p. 6771-6778.

34. Murphy, C.J. and N.R. Jana, *Controlling the aspect ratio of inorganic nanorods and nanowires.* Advanced Materials, 2002. **14**(1): p. 80-82.

35. Peng, X.G., et al., *Shape control of CdSe nanocrystals.* Nature, 2000. **404**(6773): p. 59-61.

36. Mokari, T., et al., *Formation of asymmetric one-sided metal-tipped semiconductor nanocrystal dots and rods.* Nature Materials, 2005. **4**(11): p. 855-863.

37. Hoffmann, M., et al., *3D Brownian Diffusion of Submicron-Sized Particle Clusters.* Acs Nano, 2009. **3**(10): p. 3326-3334.

38. Yin, Y.D., et al., *Formation of hollow nanocrystals through the nanoscale Kirkendall Effect.* Science, 2004. **304**(5671): p. 711-714.

39. Nan, C.Y., et al., *Size and shape control of LiFePO4 nanocrystals for better lithium ion battery cathode materials.* Nano Research, 2013. **6**(7): p. 469-477.

40. Smith, K.C., P.P. Mukherjee, and T.S. Fisher, *Columnar order in jammed LiFePO4 cathodes: ion transport catastrophe and its mitigation.* Physical Chemistry Chemical Physics, 2012. **14**(19): p. 7040-7050.

41. Hoffmann, M., et al., *Dumbbell-Shaped Polyelectrolyte Brushes Studied by Depolarized Dynamic Light Scattering.* Journal of Physical Chemistry B, 2008. **112**(47): p. 14843-14850.

42. Nelson, J., *Solar energy - Solar cells by self-assembly?* Science, 2001. **293**(5532): p. 1059-1060.

43. Korgel, B.A., et al., *Assembly and self-organization of silver nanocrystal superlattices: Ordered "soft spheres".* Journal of Physical Chemistry B, 1998. **102**(43): p. 8379-8388.

44. Kato, T., *Self-assembly of phase-segregated liquid crystal structures.* Science, 2002. **295**(5564): p. 2414-2418.

45. Cui, Y., et al., *Electrical transport through a single nanoscale semiconductor branch point.* Nano Letters, 2005. **5**(7): p. 1519-1523.

46. Colvin, V.L., A.N. Goldstein, and A.P. Alivisatos, *Semiconductor Nanocrystals Covalently Bound to Metal-Surfaces with Self-Assembled Monolayers.* Journal of the American Chemical Society, 1992. **114**(13): p. 5221-5230.

47. Bates, M.A. and D. Frenkel, *Phase behavior of two-dimensional hard rod fluids.* Journal of Chemical Physics, 2000. **112**(22): p. 10034-10041.

48. Bolhuis, P.G., et al., *Numerical study of the phase behavior of rodlike colloids with attractive interactions.* Journal of Chemical Physics, 1997. **107**(5): p. 1551-1564.

49. Savenko, S.V. and M. Dijkstra, *Phase behavior of a suspension of colloidal hard rods and nonadsorbing polymer.* Journal of Chemical Physics, 2006. **124**(23).

50. Sztrum, C.G. and E. Rabani, *Out-of-equilibrium self-assembly of binary mixtures of nanoparticles.* Advanced Materials, 2006. **18**(5): p. 565-+.

51. Kletenik-Edelman, O., et al., *Drying-mediated hierarchical self-assembly of nanoparticles: A dynamical coarse-grained approach.* Journal of Physical Chemistry C, 2008. **112**(12): p. 4498-4506.

52. Sztrum, C.G., O. Hod, and E. Rabani, *Self-assembly of nanoparticles in three-dimensions: Formation of stalagmites.* Journal of Physical Chemistry B, 2005. **109**(14): p. 6741-6747.

53. Korgel, B.A. and D. Fitzmaurice, *Small-angle x-ray-scattering study of silver-nanocrystal disorder-order phase transitions.* Physical Review B, 1999. **59**(22): p. 14191-14201.

54. Saunders, A.E., et al., *Solvent density-dependent steric stabilization of perfluoropolyether-coated nanocrystals in supercritical carbon dioxide.* Journal of Physical Chemistry B, 2004. **108**(41): p. 15969-15975.

55. Yosef, G. and E. Rabani, *Self-assembly of nanoparticles into rings: A lattice-gas model.* Journal of Physical Chemistry B, 2006. **110**(42): p. 20965-20972.

56. Maillard, M., et al., *Rings and hexagons made of nanocrystals: A Marangoni effect.* Journal of Physical Chemistry B, 2000. **104**(50): p. 11871-11877.

57. Maillard, M., L. Motte, and M.P. Pileni, *Rings and hexagons made of nanocrystals.* Advanced Materials, 2001. **13**(3): p. 200-204.

58. Stowell, C. and B.A. Korgel, *Self-assembled honeycomb networks of gold nanocrystals.* Nano Letters, 2001. **1**(11): p. 595-600.

59. Zhu, M., et al., *Numerical Study of Interaction and Aggregation of Non-Spherical Particles in Forming Li-Ion Battery Cathodes.* Journal of the Electrochemical Society, 2014. **161**(9): p. A1247-A1252.

60. Vancea, I., et al., *Front instabilities in evaporatively dewetting nanofluids.* Physical Review E, 2008. **78**(4).

61. Liu, Z.X., V. Battaglia, and P.P. Mukherjee, *Mesoscale Elucidation of the Influence of Mixing Sequence in Electrode Processing.* Langmuir, 2014. **30**(50): p. 15102-15113.

62. Liu, Z.X. and P.P. Mukherjee, *Microstructure Evolution in Lithium-Ion Battery Electrode Processing.* Journal of the Electrochemical Society, 2014. **161**(8): p. E3248-E3258.

63. Sheetz, D.P., *Formation of Films by Drying of Latex.* Journal of Applied Polymer Science, 1965. **9**(11): p. 3759-&.

64. Davis, K.E. and W.B. Russel, *An Asymptotic Description of Transient Settling and Ultrafiltration of Colloidal Dispersions.* Physics of Fluids a-Fluid Dynamics, 1989. **1**(1): p. 82-100.

65. Auzerais, F.M., R. Jackson, and W.B. Russel, *The Resolution of Shocks and the Effects of Compressible Sediments in Transient Settling.* Journal of Fluid Mechanics, 1988. **195**: p. 437-462.

66. Auzerais, F.M., et al., *The Transient Settling of Stable and Flocculated Dispersions.* Journal of Fluid Mechanics, 1990. **221**: p. 613-639.

67. Routh, A.F. and W.B. Russel, *Deformation mechanisms during latex film formation: Experimental evidence.* Industrial & Engineering Chemistry Research, 2001. **40**(20): p. 4302-4308.

68. Routh, A.F. and W.B. Zimmerman, *Distribution of particles during solvent evaporation from films.* Chemical Engineering Science, 2004. **59**(14): p. 2961-2968.

69. Routh, A.F. and W.B. Russel, *Horizontal drying fronts during solvent evaporation from latex films.* Aiche Journal, 1998. **44**(9): p. 2088-2098.

70. Routh, F. and W.B. Russel, *Horizontal drying fronts during solvent evaporation from latex films (vol 44, pg 2088, 1998).* Aiche Journal, 2002. **48**(4): p. 917-918.

71. Routh, A.F. and W.B. Russel, *Process model of latex film formation: Particle deformation.* Abstracts of Papers of the American Chemical Society, 1999. **218**: p. U621-U621.

72. Shimmin, R.G., A.J. DiMauro, and P.V. Braun, *Slow vertical deposition of colloidal crystals: A Langmuir-Blodgett process?* Langmuir, 2006. **22**(15): p. 6507-6513.

73. Trueman, R.E., et al., *Auto-stratification in drying colloidal dispersions: A diffusive model.* Journal of Colloid and Interface Science, 2012. **377**: p. 207-212.

74. Trueman, R.E., et al., *Autostratification in Drying Colloidal Dispersions: Experimental Investigations.* Langmuir, 2012. **28**(7): p. 3420-3428.

75. Atmuri, A.K., S.R. Bhatia, and A.F. Routh, *Autostratification in Drying Colloidal Dispersions: Effect of Particle Interactions.* Langmuir, 2012. **28**(5): p. 2652-2658.

76. Landau, D.P. and K. Binder, *A guide to Monte Carlo simulations in statistical physics*. 2014: Cambridge university press.

77. Niederreiter, H., et al., *Monte Carlo and quasi-Monte Carlo methods 1996: proceedings of a conference at the University of Salzburg, Austria, July 9-12, 1996*. Vol. 127. 2012: Springer Science & Business Media.

78. Niederreiter, H., *Quasi-Monte Carlo methods and pseudo-random numbers.* Bulletin of the American Mathematical Society, 1978. **84**(6): p. 957-1041.

79. Metropolis, N., et al., *Equation of state calculations by fast computing machines.* The journal of chemical physics, 1953. **21**(6): p. 1087-1092.

80. Young, W. and E. Elcock, *Monte Carlo studies of vacancy migration in binary ordered alloys: I.* Proceedings of the Physical Society, 1966. **89**(3): p. 735.

81. Bortz, A.B., M.H. Kalos, and J.L. Lebowitz, *A new algorithm for Monte Carlo simulation of Ising spin systems.* Journal of Computational Physics, 1975. **17**(1): p. 10-18.

82. Sztrum-Vartash, C.G. and E. Rabani, *Lattice Gas Model for the Drying-Mediated Self-Assembly of Nanorods.* Journal of Physical Chemistry C, 2010. **114**(25): p. 11040-11049.

83. Stupp, S.I., et al., *Supramolecular materials: Self-organized nanostructures.* Science, 1997. **276**(5311): p. 384-389.

84. Schilling, T., et al., *Monte Carlo study of hard pentagons.* Physical Review E, 2005. **71**(3).

85. Pauliac-Vaujour, E., et al., *Fingering instabilities in dewetting nanofluids.* Physical Review Letters, 2008. **100**(17).

86. Martin, C.P., M.O. Blunt, and P. Moriarty, *Nanoparticle networks on silicon: Self-organized or disorganized?* Nano Letters, 2004. **4**(12): p. 2389-2392.

87. Kletenik-Edelman, O., C.G. Sztrum-Vartash, and E. Rabani, *Coarse-grained lattice models for drying-mediated self-assembly of nanoparticles.* Journal of Materials Chemistry, 2009. **19**(19): p. 2872-2876.

88. Katsoulakis, M.A. and D.G. Vlachos, *Coarse-grained stochastic processes and kinetic Monte Carlo simulators for the diffusion of interacting particles.* Journal of Chemical Physics, 2003. **119**(18): p. 9412-9427.

89. Cardinal, C.M., et al., *Drying Regime Maps for Particulate Coatings.* Aiche Journal, 2010. **56**(11): p. 2769-2780.